Quantitative Trait Loci (QTL)-Guided Metabolic Engineering of a Complex Trait

-

Supporting Information

Matthew J. Maurer[1], Lawrence Sutardja[2], Dominic Pinel[1], Stefan Bauer[1,3], Amanda L. Muehlbauer[1], Tyler D. Ames[1,4], Jeffrey M. Skerker[1,2,5*], Adam P. Arkin[1,2,6**]

[1]Energy Biosciences Institute, University of California, Berkeley, California, United States of America.

[2]Department of Bioengineering, University of California, Berkeley, California, United States of America.

[3]Present address: Zymergen, Emeryville, California, United States of America.

[4]Present address: Phosplatin Therapeutics, New York, New York, United States of America.

[5]Biological Systems and Engineering Division, Lawrence Berkeley National Laboratory, Berkeley, California, United States of America.

[6]Environmental Genomics and Systems Biology Division, Lawrence Berkeley National Laboratory, Berkeley, California, United States of America.

[*]Corresponding author. Tel: 510-643-5692; fax: 510-642-9725; E-mail: skerker@berkeley.edu

[**]Corresponding author. Tel: 510-643-5692; fax: 510-642-9725; E-mail: aparkin@lbl.gov

Table of Contents

Selection and characterization of parent strains

We independently sequenced the genome of our JAY291^{mm} and S288C^{mm} strains and performed variant detection, to generate a set of Single Nucleotide Polymorphisms (SNPs) that would serve as markers in our QTL analysis (see **Methods**). We identified 59,325 variant sites (**File S1**), of which, ~8% were INDELs. The ~54,700 SNPs we identified is less than the previously published estimate of ~65,000[1]. A likely explanation for this discrepancy is that the estimate was derived from a region of chrXIV, which we determined to have a higher variant rate (1 per 251 bp for chrXIV) than the genome average (1 per 204 bp). Ultimately, we chose a subset of ~46,000 very high confidence SNPs between our two parent strains to follow as segregating sites in our QTL analysis (**File S2**).

Diploidization of segregant pool

Three regions were initially detected as QTLs, in addition to the 17 described in the main text. These regions, however, mapped directly or very near to the loci where we integrated the selectable marker cassettes for the magic marker selection scheme (**Figure 2A**, gray vertical lines labeled "MAT", "CAN1", and "LYP1"). The changing allele frequency at these loci was likely due to the "diploidization" of the populations, a phenomenon that has been observed by Wilkening *et al* in their own and other's BSA studies that, like us, used the SGA reporter system to generate a pool of haploids[2,3]. It has been suggested that this diploidization is likely the result of mating between the selected *MAT***a** segregants and *MAT*α cells that escape selection[2], though spontaneous mating-type switching from *MAT***a** to *MAT*α via HO-independent gene conversion with the *HML*α locus, or escaping diploids are also possible[4]. We confirmed that diploidization also occurred in our experiments with a simple halo test on 12 isolates from our initial pool, and from the control and experimental pools after selection. All 12 isolates from the initial pool tested as *MAT***a** strains, but in the control and experimental pools, only 1 and 3 out of 12 isolates, respectively, tested as *MAT***a**, the remaining tested as diploids (data not shown). Differences between allele frequency flux at QTLs in haploids and diploids depend on the specific genetics underlying a particular QTL[5], and thus the consequences of such diploidization will likely vary for each QTL. But importantly, QTLs have been successfully mapped using diploid populations, including haploid populations that diploidized during selection[2,5].

Creating a "genetic blueprint" for strain engineering using the QTL map and bRHA

Epistasis can hinder engineering[6,7]. A phenotype is not necessarily improved with each acquisition of another population-favorable allele, and the optimal strain is not necessarily a composite of the population-favorable alleles from each QTL. Evidence for this can be seen in the observed equilibriums in SNP allele frequency flux and rough/rugged fitness landscapes[5,8-12]. Underlying causes of this include sign and reciprocal sign epistasis (S/RSE), defined as epistasis resulting in the inversion of the sign of the fitness effect for one or both alleles when appearing together[9,11]. Engineering a strain by manipulating genotypes using alleles that unknowingly experience S/RSE will not yield the intended effect.

Detecting epistasis from BSA data may one day be possible, but currently it is not. For each QTL, however, the favorable allele in the population and even the amount of selective pressure acting on that allele can be determined from the magnitude and direction of the vectored SNP allele frequency flux in BSA data[5,8]. This information can provide some insight into how best to combine alleles to achieve the optimal phenotype. Reciprocal-hemizygosity analysis, however, allows one to examine the phenotypic contribution of each allele, including

contributions dependent on genetic interactions with alleles at other loci[13]. We reasoned that as a first approximation, the reciprocal-hemizygosity test can be considered a test of the allele contribution against all possible genetic backgrounds composed from the two parent strains, and this information can supplement the allele favorabilities determined from BSA data. Conceivably, epistasis could occur in a haploid between the tested allele and an allele of a second QTL, which went unnoticed in the reciprocal hemizygosity test due to a completely dominant allele at the second QTL. But for our engineering purposes, only unpredicted S/RSE is problematic (e.g. two alleles, independently beneficial, produce an overall detrimental effect when appearing together). Combining beneficial alleles that unknowingly experience positive or negative epistasis, which only magnify and mute the phenotypic effect[14], is not problematic as the net effect will be of no less benefit than that independently provided by the larger effect allele.

We determined which allelic form of each QTL subregion was favorable in the hybrid diploid strain and deduced whether that favorability manifested through a beneficial or detrimental manner by comparing hydrolysate tolerance of each reciprocal hemizygous strain to the WT hybrid diploid (**Table 1** and **Figures S9-25**). These results are described in detail in the four following subsections. Here, we summarize our bRHA results and describe how we used this information in conjunction with our BSA data to guide our strain engineering, and help avoid potentially problematic QTLs, such as those where S/RSE might occur.

We observed fixation of the JAY291 allele of QTL 04a ($04a^J$) and the S288C allele of QTL 04b ($04b^S$) in the segregant pool under hydrolysate selection (**Figure 2A**), indicating all survivors in the hydrolysate-pressured population possessed these alleles. As we determined for $04a^J$ in **Figure 2**, $04b^S$ was also favorable in both the population and in the hybrid diploid background (**Figure 2A** and **Figure S13**). Similarly, $07a^S$, $10a^J$, $12c^J$, and $14b^S$, were favorable in both the population and the hybrid diploid background, and furthermore, $10a^J$ and $12c^J$ were each beneficial to the hybrid diploid, as we saw for $04a^J$ (**Figures S14,17,20,22**). Taken together, we reasoned there was unlikely to be sign or reciprocal sign epistasis with these beneficial JAY291 alleles, and we could use them to improve hydrolysate tolerance in S288C. We further speculated that by building on S288C, we could benefit from the favorable $04a^S$, $07a^S$, and $14b^S$ QTL alleles. By contrast, there was discordance between allele favorability assessments from our BSA and bRHA data for QTLs 01a, 12a, 12b, and 16a (**Figure 2** and **Figures S9,18,19,25**). These apparent discrepancies could result from unknowingly interrogating by BSA and bRHA, two different, very tightly linked QTLs with opposite favorable alleles[15-17]. Alternatively, the discrepancies could be due to genetic background differences causing an inversion in the allele effect (i.e. S/RSE)[9-12,14,18]. In either case, trying to engineer a strain by manipulating the genotypes at such QTLs could be challenging; determining how to optimally combine the alleles of such QTLs is less straightforward, and would likely require multiple rounds of strain construction and testing. We therefore avoided these potentially problematic QTLs.

The favorable allele is beneficial to the hybrid diploid for some QTLs

In the main text we show that the JAY291 allele of QTL 04a ($04a^J$) was the favorable QTL allele in both the population as well as the hybrid diploid, and furthermore, that it was beneficial to the hybrid diploid strain (**Figure 2**). Similarly, we observed an enrichment of the JAY291 allele at QTL 10a ($10a^J$) when the segregant pool was grown in media containing 30% (vol/vol) hydrolysate (**Figure 2A**), indicating the $10a^J$ QTL allele is favorable in the population. To expedite the confirmation of QTL 10a (and other QTLs where the 95% confidence interval of the map position was larger than 10 kb), we used a larger bulk size of 5 kb, and constructed three pairs of reciprocal hemizygous strains to scan ~15 kb near the best predicted position of QTL 10a (**Figure S17**). Each of the three reciprocal hemizygous strain pairs were then phenotyped in a microplate reader growth assay using synthetic complete media lacking hydrolysate, or supplemented with various concentrations of hydrolysate. In the control condition, we observed

no difference in fitness between the reciprocal hemizygous strain pairs (**Figure S17B**). By contrast, we saw a difference in hydrolysate tolerance when the JAY291 allele of the 10a-Δ01 QTL subregion was deleted, relative to the S288C allele. This difference was modest when the hydrolysate concentration was 12% (**Figure S17C**, panel Δ01), and became more pronounced when increased to 24% (**Figure S17D**, panel Δ01). There was no relative phenotypic difference among the reciprocal hemizygous strains for the 10a-Δ03 region in either concentration of hydrolysate (**Figure S17C** and **D**, panels Δ03). These results confirmed the presence of a JAY291-favorable allele and refined its position to a relatively small region. Deleting the JAY291 allele of either the 10a-Δ01 or 10a-Δ02 regions from the hybrid diploid had a negative effect on hydrolysate tolerance (**Figure S17C**, panel Δ01, and **17D,** panels Δ02; compare green and black traces), whereas deleting the S288C allele of those regions had no effect (**Figure S17C**, panel Δ01, and **17D** panels Δ02**;** compare orange and black traces). This result indicates the JAY291 alleles at this QTL are beneficial to the hybrid diploid strain, whereas the S288C alleles are neutral.

As for QTLs 04a and 10a, we determined that the JAY291 allele of QTL 12c ($12c^J$) was favorable in the population (**Figure 2A**). We attempted to make six strains (three reciprocal hemizygous pairs) for the ~5 kb regions Δ01, Δ02, and Δ03 at QTL 12c (**Figure S20A**), but we were only able to generate both strains of the reciprocal pair for the Δ01 region; for regions Δ02 and Δ03 we could only generate a deletion of the S288C allele. Close examination of the published S288C genome and our JAY291 *de novo* genome assembly indicated that a Ty1-element insertion at the C-terminus of the *HAP1* gene was present in only the S288C background (**Figure S20A**); this explains why we failed to construct the Δ02 and Δ03 deletion strains for JAY291. We examined the phenotype of the Δ01 reciprocal pair and found that deletion of only the JAY291 allele of this region had a strong and hydrolysate-specific fitness defect (**Figure S20D**, panel Δ01). Thus, using bRHA we confirmed the presence of a JAY291 favorable allele in QTL 12c and refined its position to a small genomic region containing four genes (YLR253W, *NDL1*, YLR255C, and *HAP1*) (**Figure S20**). We also saw that the JAY291 allele of QTL 12c was beneficial to the hybrid diploid strain, whereas the S288C allele was neutral (**Figure S20D**, panel Δ01), as we had seen for QTL 10a.

In contrast to QTL 04a, QTL 10a, and QTL 12c, we observed enrichment of the S288C allele of QTL 07a (QTL $07a^S$) in the population (**Figure 2A**), indicating that for this QTL, the $07a^S$ QTL allele was the favorable QTL allele in the population. This result was confirmed by bRHA analysis (**Figure S14**). We constructed three pairs of reciprocal hemizygous strains by deleting three 5 kb regions at QTL 07a (**Figure S14A**). We saw a difference in hydrolysate tolerance at both 12% and 24% hydrolysate when deleting the S288C allele of the 07a-Δ01 region, relative to the JAY291 allele (**Figure S14C** and **D**, panels Δ01). There was no relative phenotypic difference among the reciprocal hemizygous strains for the Δ02 or Δ03 regions in either concentration of hydrolysate (**Figure S14C** and **D**, panels Δ02 and Δ03). The S288C allele corresponding to the Δ01 region is also beneficial to the hybrid diploid strain, whereas the JAY291 allele of this same region was neutral (**Figure S14D**, panel Δ01).

The unfavorable allele is detrimental to the hybrid diploid for some QTLs

The hydrolysate tolerance QTL, QTL 04b, was our strongest S288C-favorable QTL (**Figure 2A**). This QTL was also mapped with the highest resolution (95% CI of 6.1 kb). We therefore used smaller 2 kb deletion regions and surveyed the entire 95% confidence interval of the mapped position (**Figure S13A**). Phenotyping the 04b-Δ02 and 04b-Δ03 reciprocal hemizygous strains revealed that the strains deleted for the S288C allele of these regions were less fit in hydrolysate

than the strains deleted for the JAY291 allele (**Figure S13C**, panels Δ02 and Δ03). This is also true in the absence of hydrolysate (**Figure S13B**, panels Δ02 and Δ03). The hydrolysate-specific phenotype, however, became apparent when comparing the reciprocal hemizygous strains carrying deletions of the JAY291 allele of the Δ02 and Δ03 regions to the wild type hybrid diploid; there is an improvement in hydrolysate tolerance when the JAY291 allele is deleted relative to the wild type hybrid diploid (**Figure S13D** panels Δ02 and Δ03; compare green traces to black traces). These results suggest that this region is important for overall fitness, and that a JAY291 allele is detrimental in the diploid background when challenged with toxic hydrolysate.

The S288C allele of QTL 14b was the favorable QTL allele in the segregant population, as it was for QTLs 04b and 07a (**Figure 2A**). We examined QTL 14b by bRHA using 5 kb windows to scan 15 kb centered on the predicted QTL position (**Figure S22A**). The strain deleted for the S288C allele of the Δ01 region of QTL 14b was less fit in hydrolysate relative to when the JAY291 allele was deleted at the same region (**Figure S22D**, panel Δ01). This phenotypic difference manifested from a fitness improvement when the JAY291 allele of this same region was deleted (**Figure S22D**, panel Δ01). Thus, the JAY291 allele of QTL 14b is detrimental, whereas the S288C QTL allele is neutral.

For one of the identified QTLs, QTL 15b, we determined that the JAY291 QTL allele was favorable as a result of the S288C QTL allele being detrimental (**Figure S24**). We had previously observed for QTL 15b, that the JAY291 allele was favorable in the segregant population (**Figure 2A**). We assessed the 5 kb region centered on the best prediction site of QTL 15b by bRHA using deletion alleles as before. Visually, there is a very slight decrease in fitness for the reciprocal hemizygous strain carrying the ΔS288C allele, relative to the ΔJAY291 allele (**Figure S24D**, panel Δ02). To convince ourselves that this difference was real, we fit logistic growth curve models to each trial at 24% hydrolysate for these reciprocal hemizygous strains, obtained the parameter estimates from the fitted growth curve models, and then calculated the $\log_2$ ratios to determine the within-plate (i.e. within replicate experiment) relative growth differences of the reciprocal hemizygous strains ($\Delta^{JAY291}/WT^{S288C}$: $WT^{JAY291}/\Delta^{S288C}$). A one-sample t-test confirmed that the difference in hydrolysate tolerance between the $\Delta^{JAY291}/WT^{S288C}$ and the $WT^{JAY291}/\Delta^{S288C}$ reciprocal hemizygous strains of region 15b-Δ02, while small, was in fact statistically significant (**Figure S24E**, top panel).

The population-favorable allele is not always favorable in the hybrid diploid

For QTLs 12a and 12b, the S288C alleles predominated in the population (**Figure 2A**), whereas in the hybrid diploid strain, the JAY291 QTL alleles were favorable (**Figures S18** and **19**). In the case of QTL 12a, deleting the S288C allele at QTL subregion 12a-Δ03 from the hybrid diploid strain improved hydrolysate tolerance and deleting the JAY291 allele at the same locus decreased hydrolysate tolerance (**Figure S18D**, panel Δ03). These results indicate the S288C allele is detrimental to the hybrid diploid strain while the JAY291 allele is beneficial. We did not observe a decrease in hydrolysate tolerance when deleting the JAY291 allele of the neighboring QTL subregion 12a-Δ02; however, deleting the S288C allele of the 12a-Δ02 region improved hydrolysate tolerance (**Figure S18D**, panel Δ02), as we observed when deleting the S288C allele of 12a-Δ03. At the second QTL on chrXII, QTL 12b, comparison of the wild type hybrid diploid strain to the reciprocal hemizygotes carrying deletions in the 12b-Δ01 region revealed the S288C allele of QTL 12b was detrimental to the WT hybrid diploid strain, making the neutral JAY291 allele the favorable allele in the diploid strain (**Figure S19D**, panel Δ01).

There were also discrepancies between the allele favorability observed in the population and the hybrid diploid strain for two additional QTLs (QTL 01a and QTL 16a). In these cases, the JAY291 allele was favorable in the population (**Figure 2A**) but not in the wild type hybrid

diploid strain; the S288C allele was beneficial to the hybrid diploid strain when grown in hydrolysate, whereas the JAY291 allele was neutral (**Figures S9D**, panel Δ02 and **25D**, panel Δ02, respectively). Because the difference between the reciprocal hemizygous strains for the 16a-Δ02 region was very small, we once again fit growth curve models to the bRHA data, and determined that deleting the S288C did result in a statistically significant increase in lag phase, relative to deleting the JAY291 allele in the same region (**Figure S25E**, middle panel).

Haploinsufficiency as evidence for hydrolysate tolerance alleles

For QTL 13a, a visual inspection of the growth curves from the bRHA data revealed an apparent slight difference in hydrolysate tolerance between the reciprocal hemizygous strains of the 13a-Δ01 region (**Figure S21D**). This was also true for the Δ02 region of QTL 15a (**Figure S23D**). We again fit logistic growth curve models and compared the fitted parameters to assess the perceived tolerance differences between the two strains of each reciprocal hemizygous strain pair. In neither case were the differences statistically significant (data not shown). We did, however, also notice a hydrolysate-specific haploinsufficiency for both the 13a-Δ01 and 15a-Δ02 regions (**Figures S21D** and **23D**, compare black traces to green and orange traces). This haploinsufficiency indicates these regions are important for hydrolysate tolerance, and reveal hydrolysate tolerant alleles. We believe this growth data from our bRHA data of the 13a-Δ01 and 15a-Δ02 regions supports the existence of QTLs 13a and 15a identified from our BSA data (see **Figure 2A**, and **Figures S21A** and **23A**), despite our inability to measure a phenotypic difference using our microplate reader growth assay. Nevertheless, while we conclude these regions are important to hydrolysate tolerance and that both alleles are beneficial to the hybrid diploid strain, we refrain from making a determination as to which allele is favorable in the hybrid diploid strain background.

A Cas9-mediated engineering strategy for simultaneous replacement of many variants in regions of highly homologous DNA.

In light of our goal to engineer complex phenotypes into strains, we desired a method enabling the rapid replacement of many genetic variants. To this end, we sought a Cas9 strategy that allowed us to simultaneously replace many variants in large regions of highly homologous DNA, such as those we confirmed by bRHA. Recently, Horwitz and colleagues simultaneously replaced three SNPs within an ~150 bp region in *S. cerevisiae* by providing a single donor DNA and using Cas9 with two guides to excise the 150 bp region[19]. While, they do not describe this dual-guide approach in detail or provide their rationale for using two guides instead of a more standard single guide approach, we speculate their motivation came from thirty-year old yeast recombinational cloning studies, which would suggest that generating two double-strand breaks at sites flanking the targeted replacement region should be made to best ensure a complete replacement of the entire allelic region[20-22].

In spite of this thirty-year old wisdom, we decided to see if a simpler single-guide method would be sufficient in substituting many variants over relatively large genomic regions, since Horwitz and colleagues also did not compare the allele replacement efficiency of a dual-guide approach to a more standard single-guide approach. We attempted bulk variant replacements by directing Cas9 to generate a double strand break in the S288C chromosome at a single site centered in the region we wished to replace, and providing a PCR product amplified from the JAY291 genome as the donor DNA to serve in the repair of the Cas9-induced double strand break by homologous recombination (**Figure 1C-D**). We selected a Cas9-targeting sequence (23 nt sequence corresponding to a PAM site (5'-NGG-3') and the immediate upstream 20 nt protospacer sequence) within the intended bulk variant replacement region, such that there was at

least one SNP, relative to JAY291, within the 23 nt sequence, not including SNPs at the N position in the PAM (see **Methods** for more detail). We reasoned that one SNP in the targeting sequence region might prevent cleavage of the JAY291 donor DNA by Cas9, allowing the donor DNA to be used in homology directed double strand break repair. It is known that mutations in the targeting sequence, especially those which fall within the PAM sequence, can significantly reduce Cas9 cleavage[23,24]. A plasmid expressing both Cas9 and the single sgRNA was co-transformed with JAY291 donor DNA into S288C, and transformants were genotyped at every variant site within the targeted replacement region using Sanger sequencing (**Figure S3**).

We identified one isolate carrying the JAY291 allele at all intended variant sites when this single guide method was implemented (**Figure S3A**). This demonstrates that we can effectively utilize Cas9 to simultaneously replace multiple variants in regions of highly homologous DNA. However, most of the isolates had the S288C allele replaced with the JAY291 allele in only a subset of the intended variant sites, and the successfully substituted sites tended to emanate out from the Cas9 cut site. There were also isolates in which none of the variant sites had been replaced (**Figure S3A** and **B**). Overall, the frequency at which we isolated fully substituted strains using only a single sgRNA was rather low (1/10 for 04a-07^{J}, **Figure S3A,** and 0/12 for 04a-08^{J}, **Figure S3B**).

We sought to improve the effectiveness of our Cas9 approach for strain engineering by increasing the rate at which substitution occurred at all desired variant sites. We redesigned our strategy to utilize two Cas9 target sites per region in a manner analogous to the often implemented "plasmid gapping" strategy used for cloning by homologous recombination in yeast[20-22]. We reasoned that if Cas9 could be targeted to cut at the extreme ends of the desired substitution region, the incorporation of the desired alleles would be promoted by the removal of the undesired alleles (**Figure 1E**). This dual-guide approach proved to be much more successful in generating strains substituted at all intended variant sites. Efficiency approached 100% when the dual DSBs could be made such that they flanked all variant sites one wishes to replace; a situation permitted when left-most and right-most targeted variants fell within 20 bp of CCN and NGG PAM sites, respectively (**Figure 1D** and **Figure S3C**).

References

(1) Argueso, J. L., Carazzolle, M. F., Mieczkowski, P. A., Duarte, F. M., Netto, O. V. C., Missawa, S. K., Galzerani, F., Costa, G. G. L., Vidal, R. O., Noronha, M. F., Dominska, M., Andrietta, M. G. S., Andrietta, S. R., Cunha, A. F., Gomes, L. H., Tavares, F. C. A., Alcarde, A. R., Dietrich, F. S., McCusker, J. H., Petes, T. D., and Pereira, G. A. G. (2009) Genome structure of a *Saccharomyces cerevisiae* strain widely used in bioethanol production. *Genome Research 19*, 2258–2270.
(2) Wilkening, S., Lin, G., Fritsch, E. S., Tekkedil, M. M., Anders, S., Kuehn, R., Nguyen, M., Aiyar, R. S., Proctor, M., Sakhanenko, N. A., Galas, D. J., Gagneur, J., Deutschbauer, A., and Steinmetz, L. M. (2014) An evaluation of high-throughput approaches to QTL mapping in *Saccharomyces cerevisiae*. *Genetics 196*, 853–865.
(3) Ehrenreich, I. M., Torabi, N., Jia, Y., Kent, J., Martis, S., Shapiro, J. A., Gresham, D., Caudy, A. A., and Kruglyak, L. (2010) Dissection of genetically complex traits with extremely large pools of yeast segregants. *Nature 464*, 1039–1042.
(4) Singh, I., Pass, R., Togay, S. O., Rodgers, J. W., and Hartman, J. L. (2009) Stringent mating-type-regulated auxotrophy increases the accuracy of systematic genetic interaction screens with *Saccharomyces cerevisiae* mutant arrays. *Genetics 181*, 289–300.
(5) Parts, L., Cubillos, F. A., Warringer, J., Jain, K., Salinas, F., Bumpstead, S. J., Molin, M., Zia, A., Simpson, J. T., Quail, M. A., Moses, A., Louis, E. J., Durbin, R., and Liti, G. (2011) Revealing the genetic structure of a trait by sequencing a population under selection. *Genome Research 21*, 1131–1138.
(6) Hubmann, G., Mathé, L., Foulquié-Moreno, M. R., Duitama, J., Nevoigt, E., and Thevelein, J. M. (2013) Identification of multiple interacting alleles conferring low glycerol and high ethanol yield in *Saccharomyces cerevisiae* ethanolic fermentation. *Biotechnol Biofuels 6*, 87.
(7) Oud, B., van Maris, A. J. A., Daran, J.-M., and Pronk, J. T. (2012) Genome-wide analytical approaches for reverse metabolic engineering of industrially relevant phenotypes in yeast. *FEMS Yeast Research 12*, 183–196.
(8) Illingworth, C. J. R., Parts, L., Schiffels, S., Liti, G., and Mustonen, V. (2012) Quantifying Selection Acting on a Complex Trait Using Allele Frequency Time Series Data. *Molecular Biology and Evolution 29*, 1187–1197.
(9) Poelwijk, F. J., Kiviet, D. J., Weinreich, D. M., and Tans, S. J. (2007) Empirical fitness landscapes reveal accessible evolutionary paths. *Nature 445*, 383–386.
(10) Poelwijk, F. J., Tănase-Nicola, S., Kiviet, D. J., and Tans, S. J. (2011) Reciprocal sign epistasis is a necessary condition for multi-peaked fitness landscapes. *Journal of Theoretical Biology 272*, 141–144.
(11) Weinreich, D. M., Watson, R. A., and Chao, L. (2005) PERSPECTIVE: SIGN EPISTASIS AND GENETIC COSTRAINT ON EVOLUTIONARY TRAJECTORIES. *Evolution 59*, 1165–1174.
(12) Chiotti, K. E., Kvitek, D. J., Schmidt, K. H., Koniges, G., Schwartz, K., Donckels, E. A., Rosenzweig, F., and Sherlock, G. (2014) The Valley-of-Death: reciprocal sign epistasis constrains adaptive trajectories in a constant, nutrient limiting environment. *Genomics 104*, 431–437.
(13) Steinmetz, L. M., Sinha, H., Richards, D. R., Spiegelman, J. I., Oefner, P. J., McCusker, J. H., and Davis, R. W. (2002) Dissecting the architecture of a quantitative trait locus in yeast. *Nature 416*, 326–330.
(14) Phillips, P. C. (2008) Epistasis - the essential role of gene interactions in the structure and evolution of genetic systems. *Nat. Rev. Genet. 9*, 855–867.
(15) Flint, J., and Mackay, T. F. C. (2009) Genetic architecture of quantitative traits in mice, flies, and humans. *Genome Research 19*, 723–733.
(16) Mackay, T. F. C., Stone, E. A., and Ayroles, J. F. (2009) The genetics of quantitative traits:

challenges and prospects. *Nat. Rev. Genet. 10*, 565–577.
(17) Swinnen, S., Schaerlaekens, K., Pais, T., Claesen, J., Hubmann, G., Yang, Y., Demeke, M., Foulquié-Moreno, M. R., Goovaerts, A., Souvereyns, K., Clement, L., Dumortier, F., and Thevelein, J. M. (2012) Identification of novel causative genes determining the complex trait of high ethanol tolerance in yeast using pooled-segregant whole-genome sequence analysis. *Genome Research 22*, 975–984.
(18) Kvitek, D. J., and Sherlock, G. (2011) Reciprocal sign epistasis between frequently experimentally evolved adaptive mutations causes a rugged fitness landscape. *PLoS Genet 7*, e1002056.
(19) Horwitz, A. A., Walter, J. M., Schubert, M. G., Kung, S. H., Hawkins, K., Platt, D. M., Hernday, A. D., Mahatdejkul-Meadows, T., Szeto, W., Chandran, S. S., and Newman, J. D. (2015) Efficient Multiplexed Integration of Synergistic Alleles and Metabolic Pathways in Yeasts via CRISPR-Cas. *Cell Systems 1*, 88–96.
(20) Ma, H., Kunes, S., Schatz, P. J., and Botstein, D. (1987) Plasmid construction by homologous recombination in yeast. *Gene 58*, 201–216.
(21) Orr-Weaver, T. L., and Szostak, J. W. (1983) Yeast recombination: the association between double-strand gap repair and crossing-over. *Proc. Natl. Acad. Sci. U.S.A. 80*, 4417–4421.
(22) Orr-Weaver, T. L., Szostak, J. W., and Rothstein, R. J. (1983) Genetic applications of yeast transformation with linear and gapped plasmids. *Meth. Enzymol. 101*, 228–245.
(23) Hsu, P. D., Scott, D. A., Weinstein, J. A., Ran, F. A., Konermann, S., Agarwala, V., Li, Y., Fine, E. J., Wu, X., Shalem, O., Cradick, T. J., Marraffini, L. A., Bao, G., and Zhang, F. (2013) DNA targeting specificity of RNA-guided Cas9 nucleases. *Nat. Biotechnol. 31*, 827–832.
(24) Pattanayak, V., Lin, S., Guilinger, J. P., Ma, E., Doudna, J. A., and Liu, D. R. (2013) High-throughput profiling of off-target DNA cleavage reveals RNA-programmed Cas9 nuclease specificity. *Nat. Biotechnol. 31*, 839–843.
(25) Rep, M., Proft, M., Remize, F., Tamás, M., Serrano, R., Thevelein, J. M., and Hohmann, S. (2001) The *Saccharomyces cerevisiae* Sko1p transcription factor mediates HOG pathway-dependent osmotic regulation of a set of genes encoding enzymes implicated in protection from oxidative damage. *Mol. Microbiol. 40*, 1067–1083.
(26) Zheng, D.-Q., Wang, P.-M., Chen, J., Zhang, K., Liu, T.-Z., Wu, X.-C., Li, Y.-D., and Zhao, Y.-H. (2012) Genome sequencing and genetic breeding of a bioethanol *Saccharomyces cerevisiae* strain YJS329. *BMC Genomics 13*, 479.

Supporting Information Figure Legends

Figure S1 JAY291 is more tolerant to hydrolysate than S288C. (**A**-**E**) Growth curves from three single colony purified isolates of JAY291^{mm} (APA5026, APA5027, APA5028) and S288C^{mm} (APA5029, APA5030, APA5031) in synthetic media supplemented with dilute-acid pretreated hydrolysate (DAH) at 0% (**A**), 15% (**B**), 30% (**C**), 45% (**D**), and 60% (vol/vol) (**E**). Growth curve data was generated by measuring optical density in 45-minute intervals for each strain cultured anaerobically in 48-well microplates using a Beckman DTX880 plate reader. Lines represent traces of the mean optical density (OD) from at least three biological replicates. Error bars in **A**-**E** indicate one standard deviation. (**F**) Anaerobic batch fermentations of JAY291^{mm} and S288C^{mm} (APA5026 and APA5030, respectively, the parent strains of the QTL cross) in 30% (vol/vol) DAH. Batch fermentations were performed in a DASGIP bioreactor with pH maintained at 5.5 with one-sided pH control.

Figure S2 Population growth rate increased over time for both control (no hydrolysate) and experimental (30% (vol/vol) hydrolysate) continuous-culture conditions during segregant pool enrichment. During QTL-mapping (**Figure 2A**), culture density (OD) of the populations grown in synthetic media supplemented with 0% (vol/vol) hydrolysate (light blue) and in 30% (vol/vol) hydrolysate (light red) were allowed to reach 5 OD units, at which point the bioreactors entered the turbidostat phase. During the turbidostat phase, the culture density was held constant at 5 OD units by pumping in fresh media and pumping out culture at the necessary rates. Rates of fresh media addition reflect the growth rates of the cultures, and are determined from the volume of fresh media pumped (mL) into the bioreactor vessels (0% and 30% (vol/vol) hydrolysate, dark blue and dark red curves, respectively) as a function of time.

Figure S3 Genotypes of transformants from Cas9-mediated bulk variant replacements. (**A**-**B**) The single-guide Cas9-mediated bulk variant replacement method produces transformants with varying subregion replacements. The S288C alleles were replaced with JAY291 alleles at 04a-07 and 04a-08 using the single-guide method. (**C**) The dual-guide Cas9-mediate bulk variant replacement success rate can approach 100%. A dual-guide Cas9-mediated bulk variant replacement was performed to replace the S288C alleles with the JAY291 alleles at 12c-02. The bulk variant replacement regions (pink hashed bars) were PCR amplified from the JAY291 genome to serve as the donor DNA. Cas9-target sites (yellow highlighted regions, comprised of a PAM and the 20 nucleotides upstream sequence) and the Cas9-induced DSB positions (vertical dark yellow lines within yellow highlighted regions) are indicated. Transformants were Sanger sequenced to determine the genotype at each variant site. Red, black, and grey "x" symbols signify the genotype at known SNP positions (JAY291, S288C, or undetermined, respectively).

Figure S4 QTL fine-mapping using the single-guide Cas9-mediated bulk variant replacement method reveals variants in the *SFA1* promoter region important for hydrolysate tolerance. (**A**) Genotypes of five different full and partial bulk variant replacement strains for QTL 04a, generated by the single-guide Cas9-mediated bulk variant replacement method. Red and black "x" symbols signify JAY291 and S288C alleles, respectively, at known SNP sites. Donor DNA (red bars, "Donor DNA 04a-07^{J}" and "Donor DNA 04a-08^{J}"), containing the JAY291 alleles at variant sites within bRHA-confirmed regions (green hashed bars, Δ07 and Δ08), were generated by PCR and used to replace S288C alleles in the S288C genome. Transformants were Sanger sequenced to determine the genotype at each variant site. Genotypes at SNP sites for JAY291 and S288C are provided as a reference. Gene ORFs (green arrows) and known *SFA1*-promoter elements (AP-1 binding sites at -409/-403 and -234/-228, Cre element at -168/-161[25], vertical gray lines), and a T→C SNP at -176 that creates an Msn2/4 binding site[26] (vertical dashed red line) are also indicated. The region spanning substituted variant sites common in the three improved strains is highlighted yellow. (**B**-**L**) Growth curves for JAY291, S288C, and allele-

substituted strains (see legend for color scheme and panel **A** for genotype), grown anaerobically in microplates in synthetic media supplemented with 0% (**B**-**F**), 24% (**G**-**K**), or 30% (vol/vol) hydrolysate (DAH) (**L**). Mean optical densities (OD) were calculated from at least three biological replicates, and traces of mean OD were plotted as a function of time. Error bars represent one standard deviation. Means and standard deviations reported for JAY291 and S288C were calculated using only trials performed in the same microplates as the bulk variant replacement strains appearing in the same plots. Growth curves in **G**-**L** and bar plots in **Figure 3B** and **C** were generated from the same data. The same JAY291 and S288C data is plotted on multiple graphs for ease of comparison (**B**-**F** and **G**-**K**).

Figure S5 The 10a-02$^{S\rightarrow J}$ bulk variant replacement improves S288C hydrolysate tolerance. (**A**) Genotypes of full bulk variant replacement strains for QTL 10a, generated by the dual-guide Cas9-mediated bulk variant replacement method. Red and black "x" symbols signify JAY291 and S288C alleles, respectively, at known SNP sites. Donor DNA (red bars, "Donor DNA 10a-01^{J}" and "Donor DNA 10a-02^{J}"), containing the JAY291 alleles at variant sites within bRHA-confirmed regions (green hashed bars, Δ01 and Δ02), were generated by PCR and used to replace S288C alleles in the S288C genome. Transformants were Sanger sequenced to determine the genotype at each variant site. Genotypes at SNP sites for JAY291 and S288C are provided as a reference. The best predicted position for QTL 10a is indicated (vertical gray line). (**B**-**C**) Growth curves for JAY291, S288C, and allele-substituted strains (see legend for color scheme and panel **A** for genotype), grown anaerobically in microplates in synthetic media supplemented with 0% (**B**) or 18% (vol/vol) hydrolysate (DAH) (**C**). Mean optical densities (OD) were calculated from at least three biological replicates, and traces of mean OD were plotted as a function of time. Error bars represent one standard deviation. Means and standard deviations reported for JAY291 and S288C were calculated using only trials performed in the same microplates as the bulk variant replacement strains appearing in the same plots. Growth curves in **C** and bar plots in **Figure 4A** were generated from the same data.

Figure S6 Multiple genetic changes in *HAP1* at QTL 12c are required to improve hydrolysate tolerance of S288C. (**A**) Genotypes of full bulk variant replacement strains for QTL 12c, generated by the dual-guide Cas9-mediated bulk variant replacement method. Red and black "x" symbols signify JAY291 and S288C alleles, respectively, at known SNP sites. Donor DNA (red bars, "Donor DNA 12c-01^{J}", "Donor DNA 12c-02^{J}", and "Donor DNA 12c-04^{J}"), containing the JAY291 alleles at variant sites within bRHA-confirmed regions (green hashed bars, Δ01), were generated by PCR and used to replace S288C alleles in the S288C genome. Transformants were Sanger sequenced to determine the genotype at each variant site. Genotypes at SNP sites for JAY291 and S288C are provided as a reference. The best predicted position for QTL 12c is indicated (vertical gray line). The YLRWTy1-3 transposon in S288C is absent in JAY291^{1}, resulting in a large INDEL (black horizontal line in the 12c-04 region). (**B**-**I**) Growth curves for JAY291, S288C, and allele-substituted strains (see legend for color scheme and panel **A** for genotype), grown anaerobically in microplates in synthetic media supplemented with 0% (**B**), 18% (**C**-**G**), 24% (**H**), or 30 % (vol/vol) dilute-acid pretreated hydrolysate (DAH) (**I**). Mean optical densities (OD) were calculated from at least three biological replicates, and traces of mean OD were plotted as a function of time. Error bars represent one standard deviation. Means and standard deviations reported for JAY291 and S288C were calculated using only trials performed in the same microplates as the bulk variant replacement strains appearing in the same plots. Growth curves in **I** and bar plots in **Figure 4C** were generated from the same data.

Figure S7 Combining bulk variant replacements provides incremental improvements in hydrolysate tolerance. (**A**-**C**) Growth curves of JAY291, S288C, and engineered strains carrying combined bulk variant replacements, grown anaerobically in microplates in synthetic media supplemented with with 30% (**A** and **B**), or 38% (vol/vol) dilute-acid pretreated hydrolysate

(DAH) (**C**). Mean optical densities (OD) were calculated from at least three biological replicates, and traces of mean OD were plotted as a function of time. Error bars represent one standard deviation. Means and standard deviations reported for JAY291 and S288C were calculated using only trials performed in the same microplates as the bulk variant replacement strains appearing in the same plots. Growth curves in **A**, **B**, and **C**, and bar plots in **Figure 4C**, **D**, and **E**, respectively, were generated from the same data.

Figure S8 QTL-guided metabolic engineering results in a strain with a superior phenotype to both parents. (**A**-**D**) Growth curves of the wild type parents JAY291, S288C, and the engineered strains "S288C+12cX3^{J}", and "6-swap" (see legend for color coding and genotype). Strains were grown anaerobically in microplates (**A**-**D**) or a DASGIP fermentation system (**E**-**H**). Growth curve data for synthetic media without hydrolysate (**A**), or synthetic media supplemented with 18% (**B**), 24% (**C**), or (**D**) 30% (vol/vol) dilute-acid pretreated hydrolysate (DAH) are shown. In **A**-**D**, mean optical densities (OD) were calculated from at least three biological replicates, and traces of mean OD were plotted as a function of time. Error bars represent one standard deviation. Means and standard deviations reported for JAY291 and S288C were calculated using only trials performed in the same microplates as the bulk variant replacement strains appearing in the same plots. (**E**-**H**) Fermentation profiles for JAY291, S288C, and the engineered strains S288C+12cX3^{J}, and 6-swap (see legend for color coding and genotype). Growth (**E**-**H**, top panels), glucose consumption and ethanol production (**E**-**H**, bottom panels) from four independent replicate experiments using synthetic media supplemented with 40% DAH are shown. Strains were grown anaerobically in a DASGIP fermentation system. Data from **Figure 5A** and **B** is also shown in **G** for ease of comparison.

Figures S9-**S25** Bulk Reciprocal Hemizygosity Analysis of the hydrolysate tolerance QTLs. (**A**) An ~15 kb window surrounding each indicated QTL, diagramming the best predicted position of the QTL (vertical grey line), SNP sites between JAY291 and S288C (grey "x" symbols), genes (arrows) within the window, and the regions deleted for bRHA (green hashed boxes). (**B**-**D**) Anaerobic microplate growth curves of the wild type hybrid diploid (WT^{JAY291}/WT^{S288C}) strain and reciprocal hemizygous strains ($\Delta^{JAY291}/WT^{S288C}$ and $WT^{JAY291}/\Delta^{S288C}$) in synthetic media without dilute-acid pretreated hydrolysate (0% DAH) (**B**), or synthetic media supplemented with 12% (**C**) or 24% (vol/vol) DAH (**D**). Reciprocal hemizygous strain pairs were constructed for each bRHA deletion region (green hashed boxes in **A**). Traces of mean culture densities, calculated from at least three biological replicates, are plotted as a function of time. Error bars indicate one standard deviation. (**E**) (**Figures S24** and **S25** only) Relative growth within the reciprocal hemizygous strain pair. Logistic growth curve models were fit (**Methods**) to each trial performed at 24% (vol/vol) hydrolysate. For each reciprocal hemizygous strain pair, the ratios ($\Delta^{JAY291}/WT^{S288C}$:$WT^{JAY291}/\Delta^{S288C}$) of the fitted growth model parameter estimates were calculated from trials within the same microplate, and $\log_2$ transformed. The means of the $\log_2$-transformed ratios are plotted. Error bars represent 95% confidence intervals calculated from the t-distribution. Reciprocal hemizygous strains with statistically significant differences within the strain pair are indicated (*; $p<0.05$ by Welch's t-test).

Supporting Information Tables

Table S1 Map positions and confidence intervals for hydrolysate tolerance QTLs calculated from BSA data

QTL	Chromosome*	Calculated Peak*	95% CI Begin*	95% CI End*	95% CI Length (bp)
QTL 01a	1	202591	185900	227900	42000
QTL 02a	2	116283	17600	269900	252300
QTL 02b	2	432914	22000	671600	649600
QTL 04a	4	157825	153900	160400	6500
QTL 04b	4	1056916	1054800	1060900	6100
QTL 07a	7	979924	839200	1043000	203800
QTL 08a	8	395587	12000	416800	404800
QTL 09a	9	109514	37700	160000	122300
QTL 10a	10	658546	644400	671800	27400
QTL 12a	12	53908	3900	180600	176700
QTL 12b	12	412996	48500	493900	445400
QTL 12c	12	650899	619600	685000	65400
QTL 13a	13	765711	60100	792200	732100
QTL 14b	14	704446	555100	738400	183300
QTL 15a	15	176463	54400	213000	158600
QTL 15b	15	619589	33300	707000	673700
QTL 16a	16	97268	7100	135400	128300

* S288C chromosome position is indicated for the Calculated Peak and the boundaries of the 95% confidence interval.

Table S2 Yeast strains used in this study. Please see attached Excel file.

Table S3 Oligonucleotides used in this study. Please see attached Excel file.

Table S4 sgRNA/Cas9 plasmids used in this study.

APA Record Number	Plasmid Name	Usage	Target Region	Single- or Dual-guide	Oligos used in plasmid construction
APA4014	pCASp3	Cas9 bulk variant replacement	04a-07[s]	Single	DPCas005, DPCas006
APA4019	pCASp8	Cas9 bulk variant replacement	04a-08[s]	Single	DPCas015, DPCas016
APA5719	pCASdg7	Cas9 bulk variant replacement	10a-01[s]	Dual	oMM0671, oMM0672, oMM0673, oMM0674
APA4095	pCASdg3	Cas9 bulk variant replacement	10a-02[s]	Dual	DPCas046, DPCas047, DPCas048, DPCas049
APA5720	pCASdg8	Cas9 bulk variant replacement	12c-01[s]	Dual	oMM0675, oMM0676, oMM0677, oMM0678
APA4096	pCASdg4	Cas9 bulk variant replacement	12c-02[s]	Dual	DPCas052, DPCas053, DPCas054, DPCas055
APA5736	pCASdg14	Cas9 bulk variant replacement	12c-04[s]	Dual	oMM0887, oMM0888, oMM0889, oMM0890

Figure S1

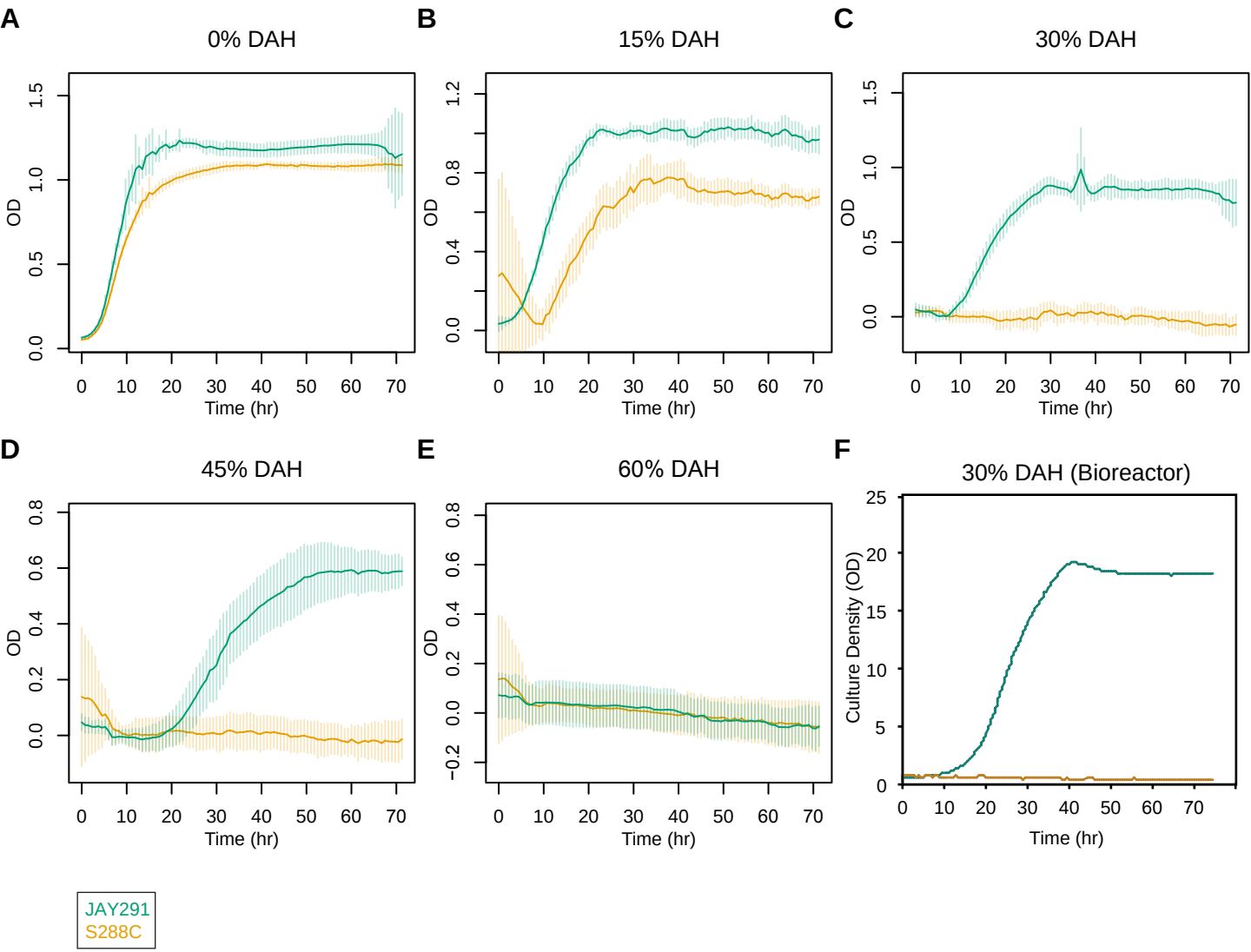
A
0% DAH
B
15% DAH
C
30% DAH
D
45% DAH
E
60% DAH
F
30% DAH (Bioreactor)
OD
Culture Density (OD)
Time (hr)
JAY291
S288C

Figure S2

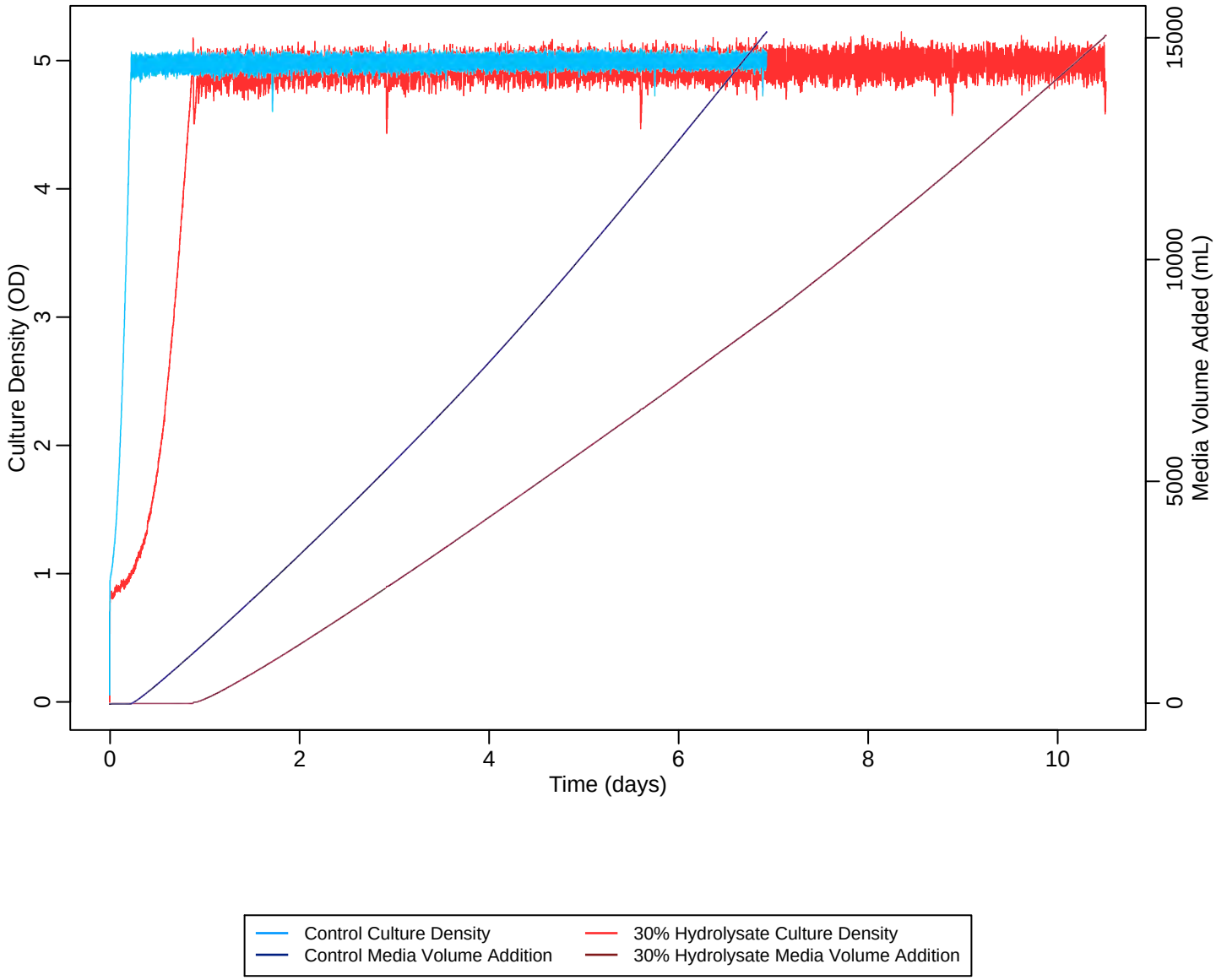
Culture Density (OD)
Media Volume Added (mL)
Time (days)
0
1
2
3
4
5
0
5000
10000
15000
0
2
4
6
8
10
Control Culture Density
Control Media Volume Addition
30% Hydrolysate Culture Density
30% Hydrolysate Media Volume Addition

Figure S3

A

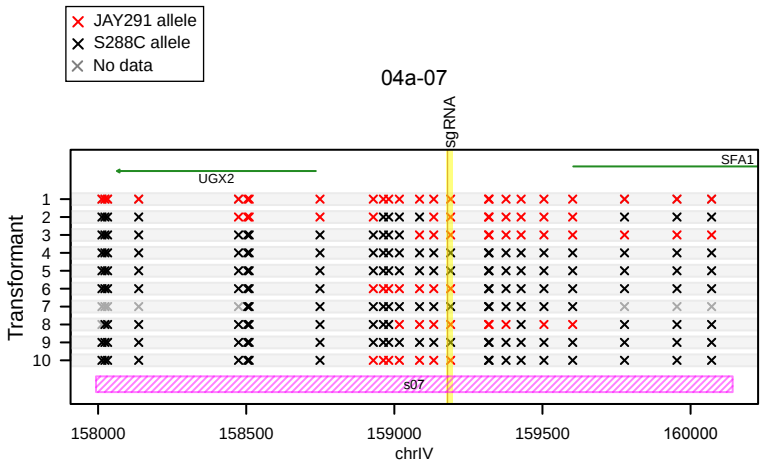

B

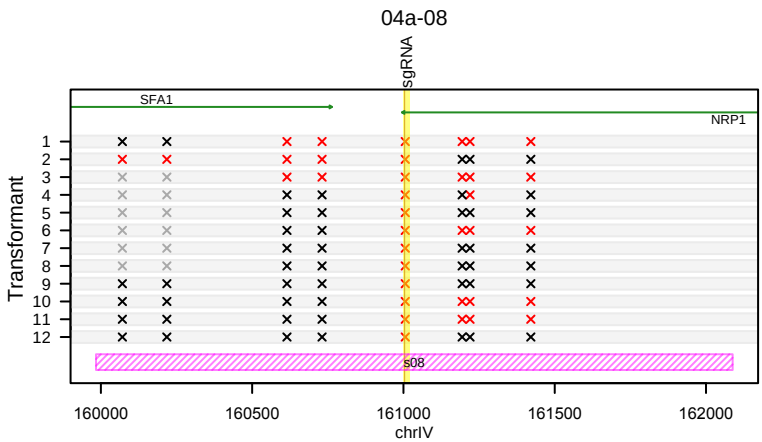

C

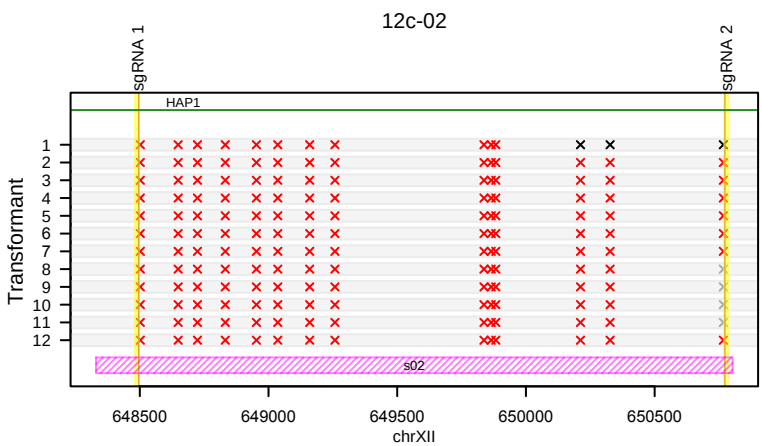

Figure S4

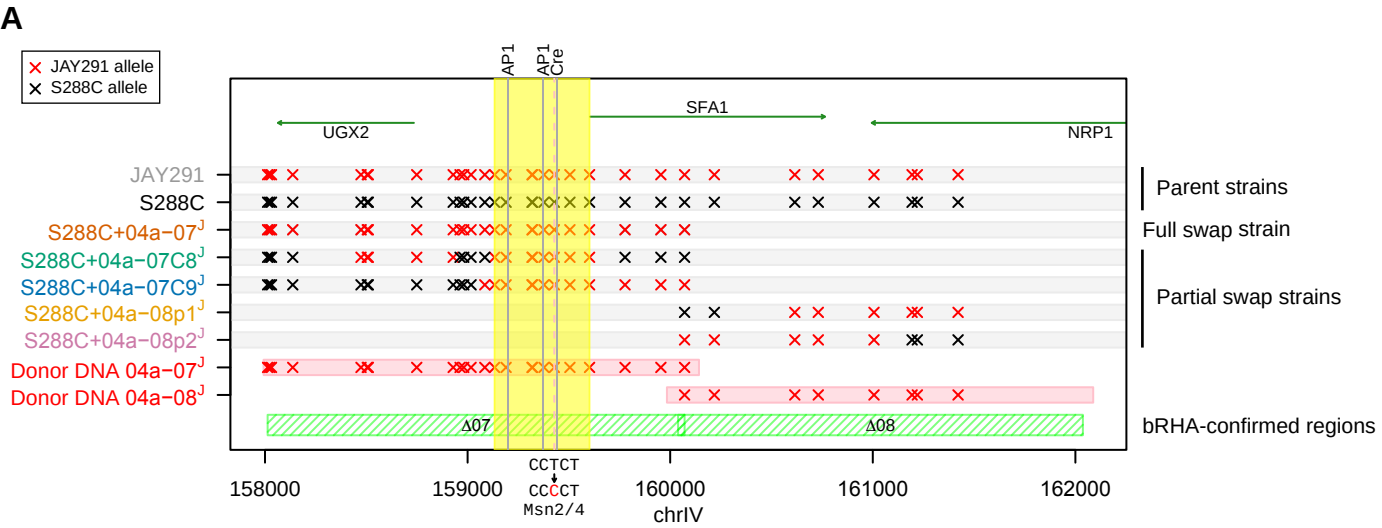
A
JAY291 allele
S288C allele
AP1
AP1 Cre
UGX2
SFA1
NRP1
JAY291
S288C
S288C+04a−07J
S288C+04a−07C8J
S288C+04a−07C9J
S288C+04a−08p1J
S288C+04a−08p2J
Donor DNA 04a−07J
Donor DNA 04a−08J
Δ07
Δ08
Parent strains
Full swap strain
Partial swap strains
bRHA-confirmed regions
158000
159000
160000
161000
162000
chrIV
CCTCT
CCCCT
Msn2/4

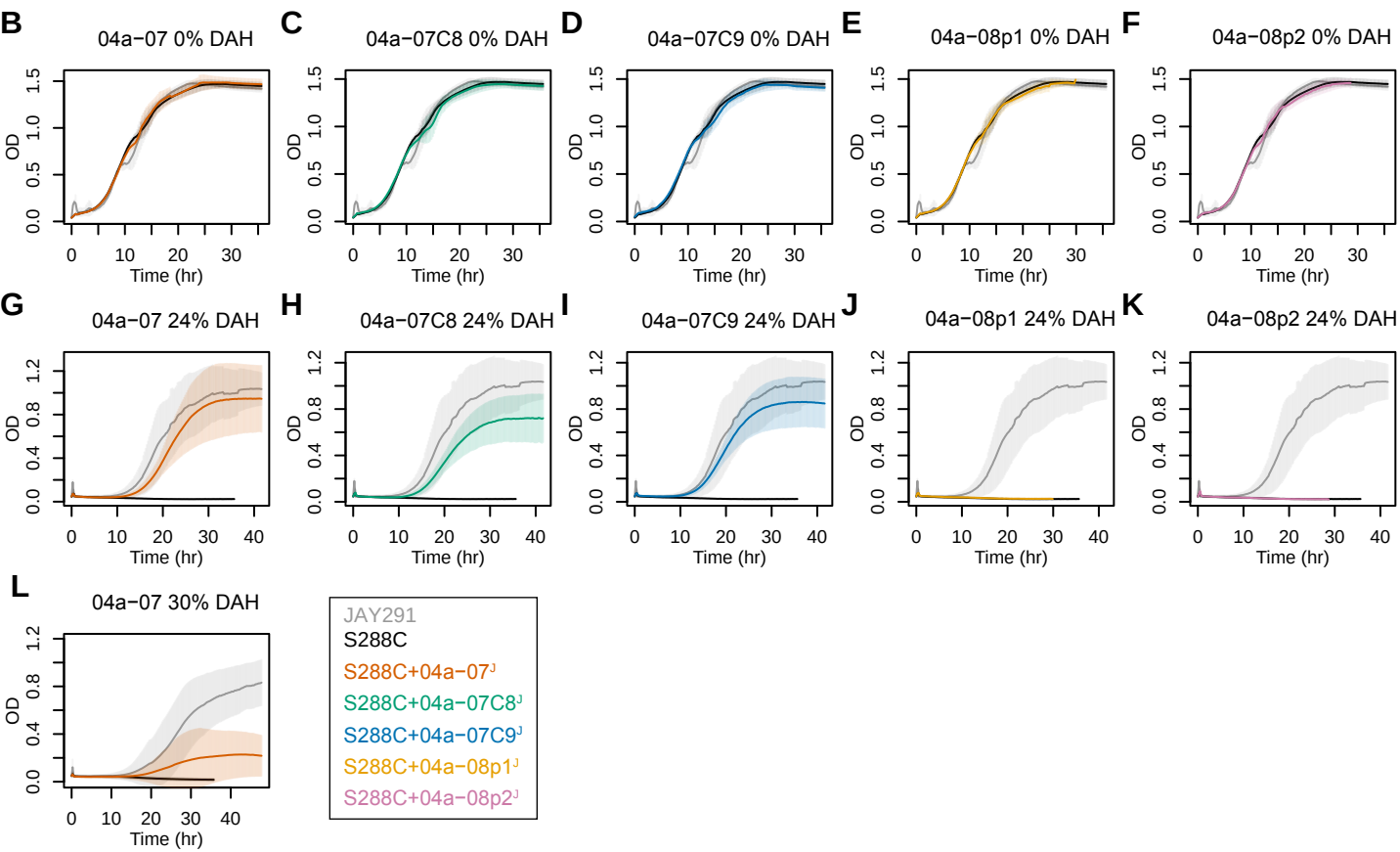
B
04a−07 0% DAH
C
04a−07C8 0% DAH
D
04a−07C9 0% DAH
E
04a−08p1 0% DAH
F
04a−08p2 0% DAH
G
04a−07 24% DAH
H
04a−07C8 24% DAH
I
04a−07C9 24% DAH
J
04a−08p1 24% DAH
K
04a−08p2 24% DAH
L
04a−07 30% DAH
OD
Time (hr)
JAY291
S288C
S288C+04a−07J
S288C+04a−07C8J
S288C+04a−07C9J
S288C+04a−08p1J
S288C+04a−08p2J

Figure S5

A

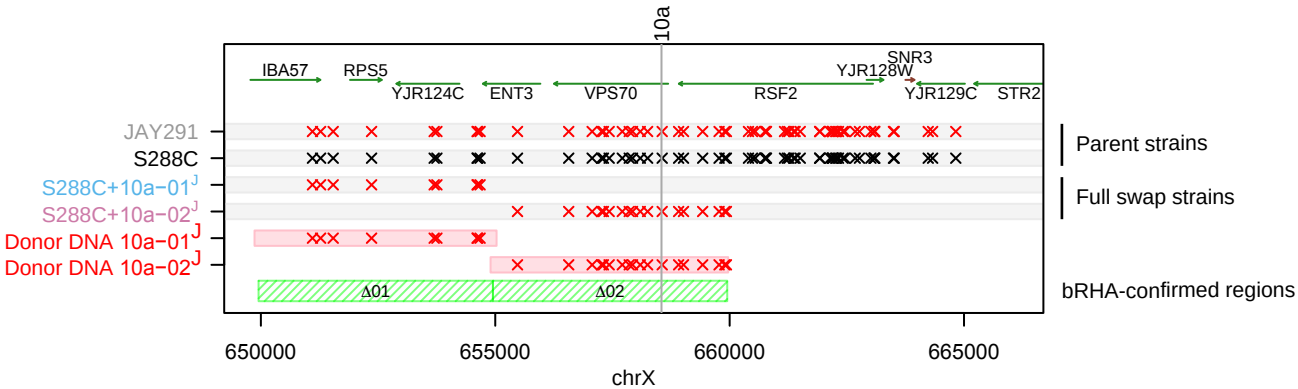

B

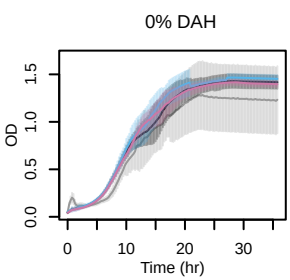

C

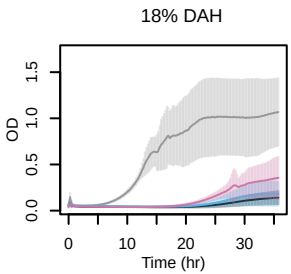

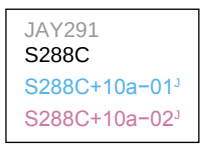

Figure S6

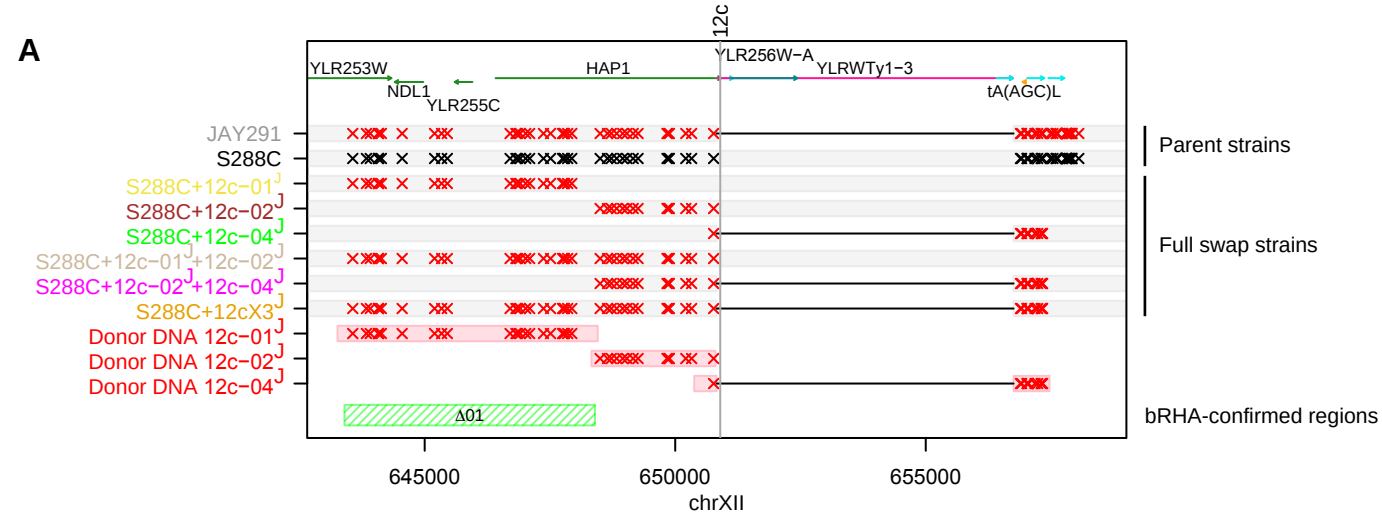
A
12c
YLR253W
NDL1
YLR255C
HAP1
YLR256W-A
YLRWTy1-3
tA(AGC)L
JAY291
S288C
S288C+12c-01J
S288C+12c-02J
S288C+12c-04J
S288C+12c-01J+12c-02J
S288C+12c-02J+12c-04J
S288C+12cX3J
Donor DNA 12c-01J
Donor DNA 12c-02J
Donor DNA 12c-04J
Δ01
Parent strains
Full swap strains
bRHA-confirmed regions
645000
650000
655000
chrXII

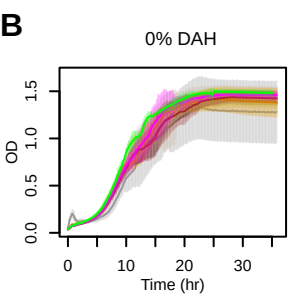
B
0% DAH
OD
Time (hr)

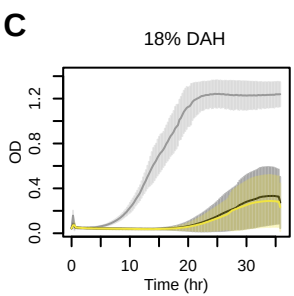
C
18% DAH
OD
Time (hr)

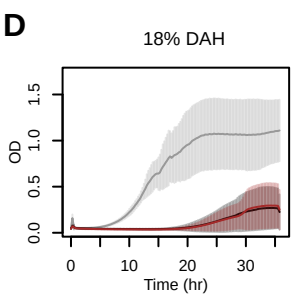
D
18% DAH
OD
Time (hr)

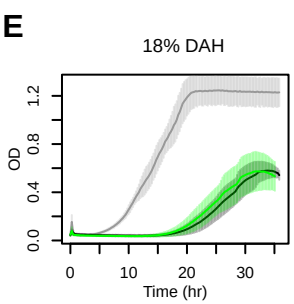
E
18% DAH
OD
Time (hr)

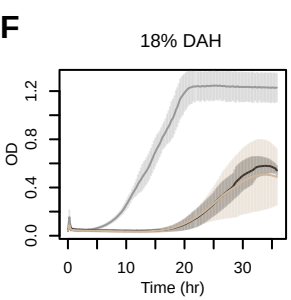
F
18% DAH
OD
Time (hr)

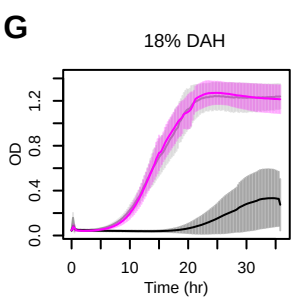
G
18% DAH
OD
Time (hr)

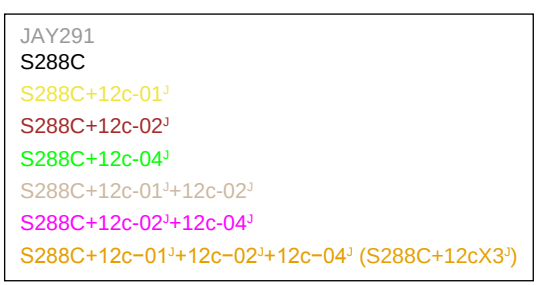
JAY291
S288C
S288C+12c-01J
S288C+12c-02J
S288C+12c-04J
S288C+12c-01J+12c-02J
S288C+12c-02J+12c-04J
S288C+12c-01J+12c-02J+12c-04J (S288C+12cX3J)

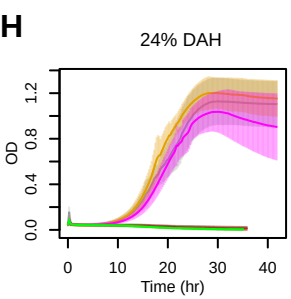
H
24% DAH
OD
Time (hr)

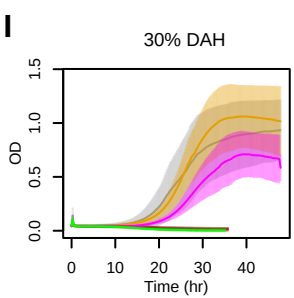
I
30% DAH
OD
Time (hr)

Figure S7

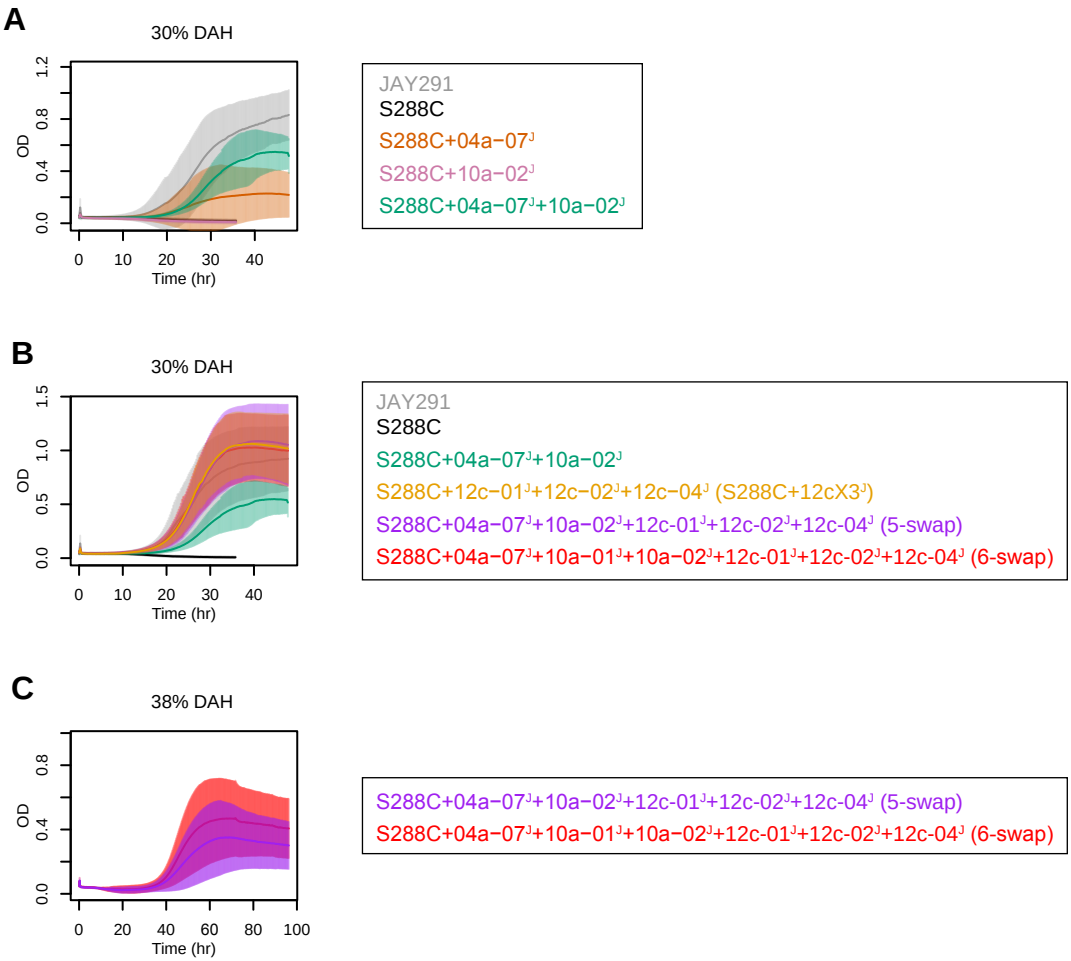
A
30% DAH
OD
Time (hr)
JAY291
S288C
S288C+04a−07J
S288C+10a−02J
S288C+04a−07J+10a−02J
B
30% DAH
OD
Time (hr)
JAY291
S288C
S288C+04a−07J+10a−02J
S288C+12c−01J+12c−02J+12c−04J (S288C+12cX3J)
S288C+04a−07J+10a−02J+12c-01J+12c-02J+12c-04J (5-swap)
S288C+04a−07J+10a−01J+10a−02J+12c-01J+12c-02J+12c-04J (6-swap)
C
38% DAH
OD
Time (hr)
S288C+04a−07J+10a−02J+12c-01J+12c-02J+12c-04J (5-swap)
S288C+04a−07J+10a−01J+10a−02J+12c-01J+12c-02J+12c-04J (6-swap)

Figure S8

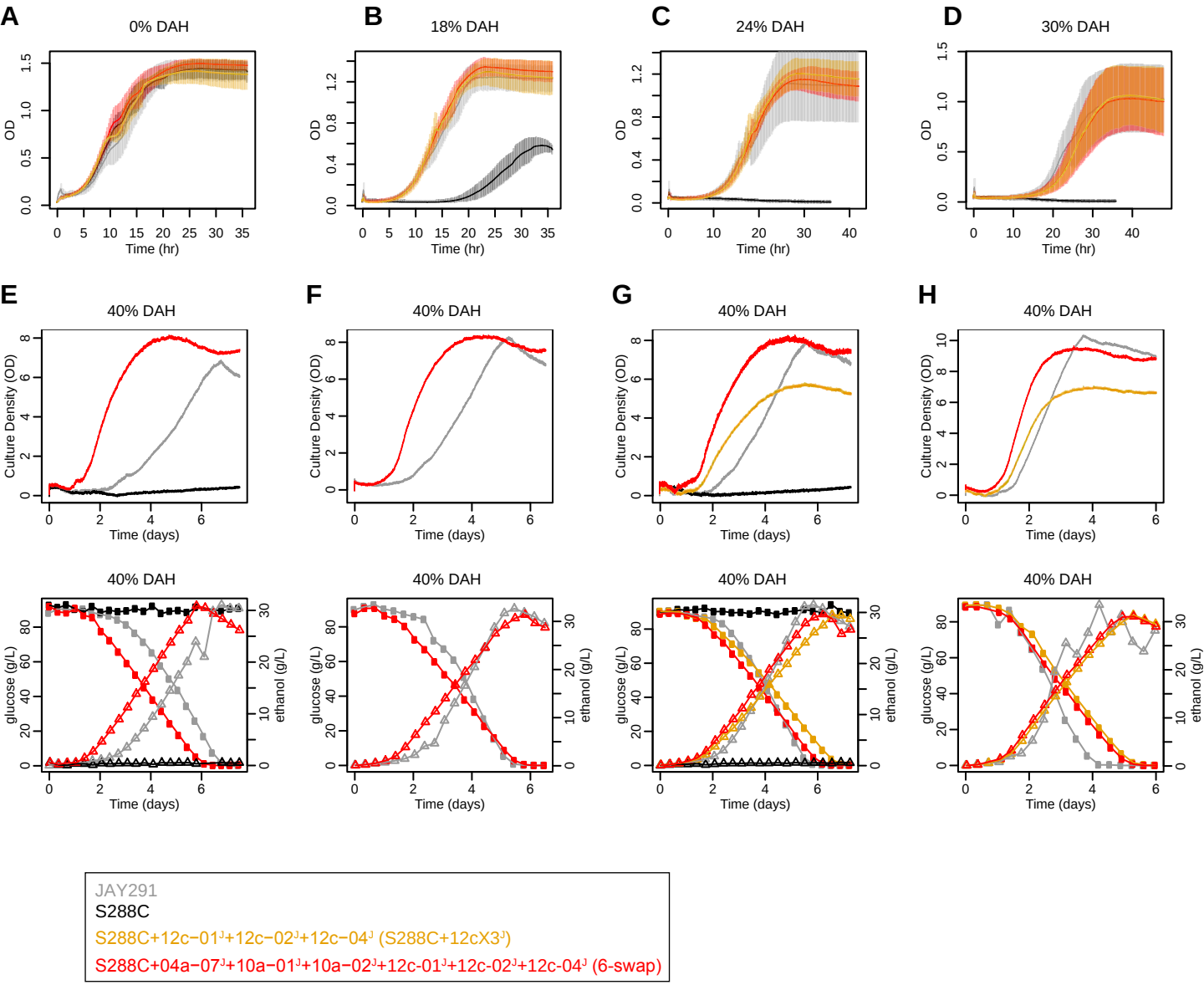

JAY291
S288C
S288C+12c−01^{J}+12c−02^{J}+12c−04^{J} (S288C+12cX3^{J})
S288C+04a−07^{J}+10a−01^{J}+10a−02^{J}+12c-01^{J}+12c-02^{J}+12c-04^{J} (6-swap)

Figure S9

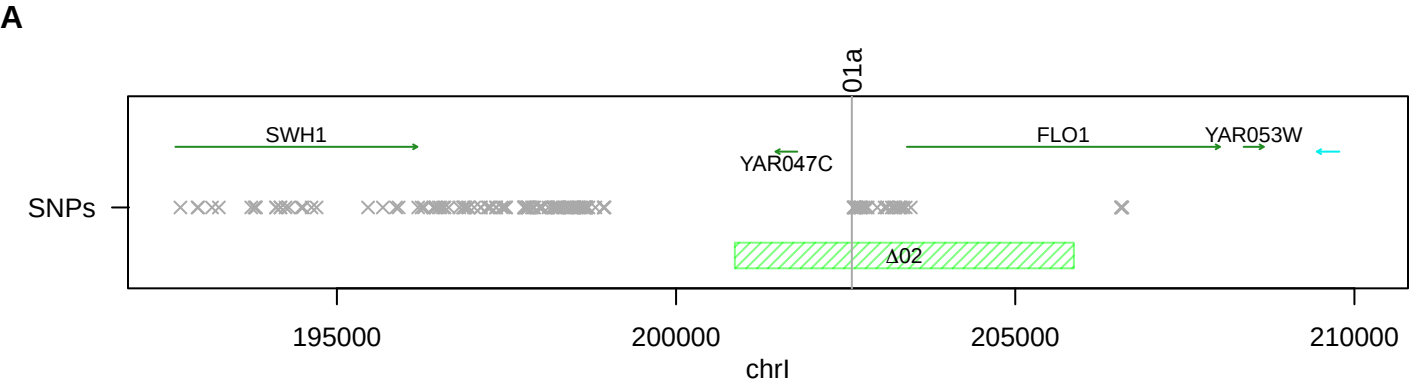
A
01a
SWH1
YAR047C
FLO1
YAR053W
SNPs
Δ02
195000
200000
205000
210000
chrI

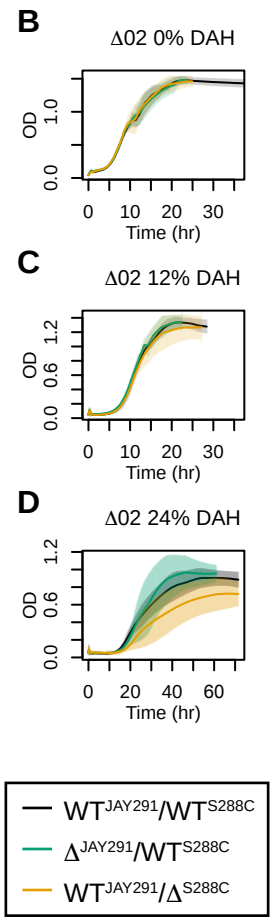
B
Δ02 0% DAH
OD
0.0
1.0
0
10
20
30
Time (hr)
C
Δ02 12% DAH
OD
0.0
0.6
1.2
0
10
20
30
Time (hr)
D
Δ02 24% DAH
OD
0.0
0.6
1.2
0
20
40
60
Time (hr)
WT^JAY291/WT^S288C
Δ^JAY291/WT^S288C
WT^JAY291/Δ^S288C

Figure S10

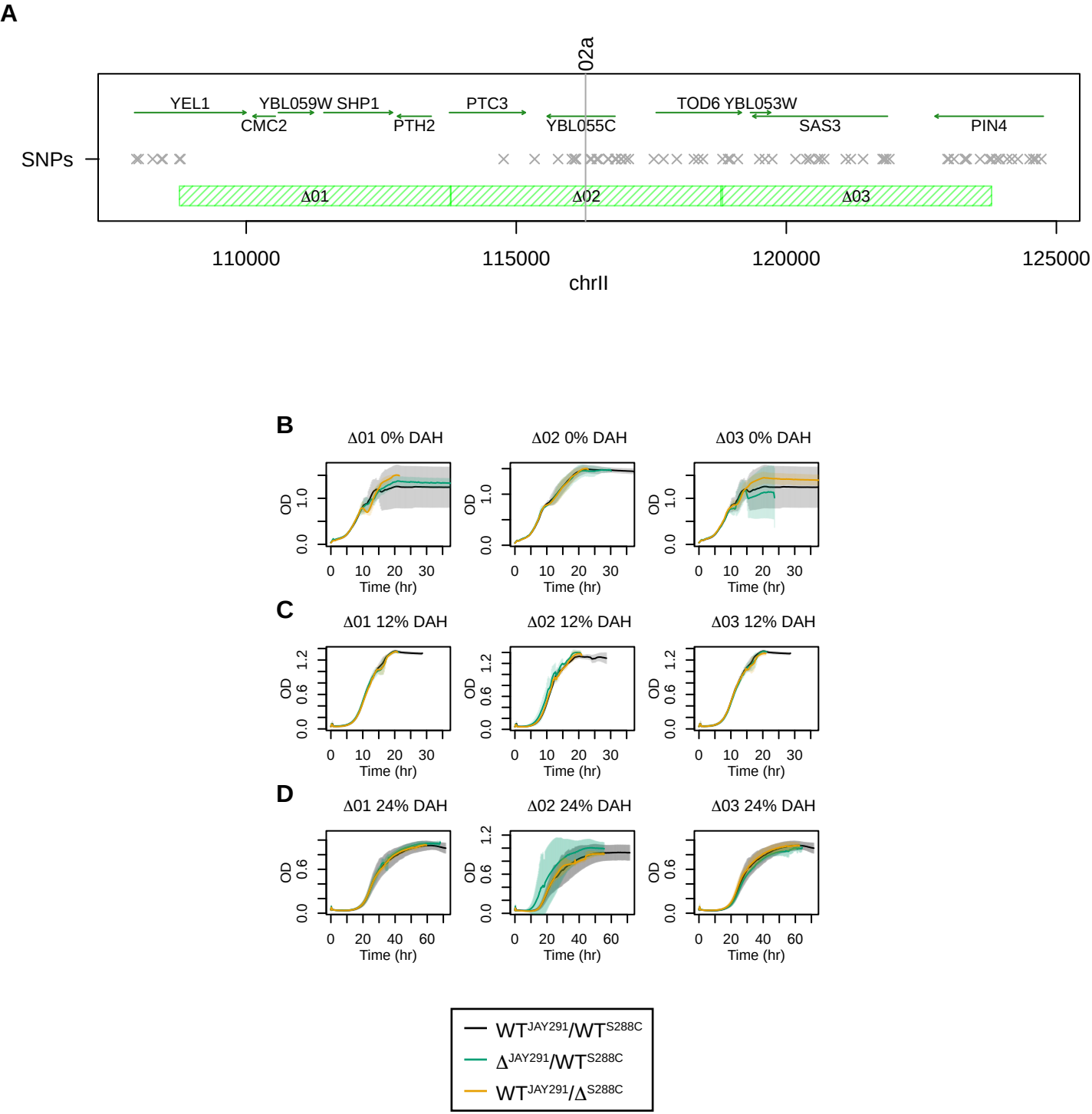
A
02a
YEL1
YBL059W
SHP1
PTC3
TOD6
YBL053W
CMC2
PTH2
YBL055C
SAS3
PIN4
SNPs
Δ01
Δ02
Δ03
110000
115000
120000
125000
chrII
B
Δ01 0% DAH
Δ02 0% DAH
Δ03 0% DAH
C
Δ01 12% DAH
Δ02 12% DAH
Δ03 12% DAH
D
Δ01 24% DAH
Δ02 24% DAH
Δ03 24% DAH
OD
Time (hr)
WT^JAY291/WT^S288C
Δ^JAY291/WT^S288C
WT^JAY291/Δ^S288C

Figure S11

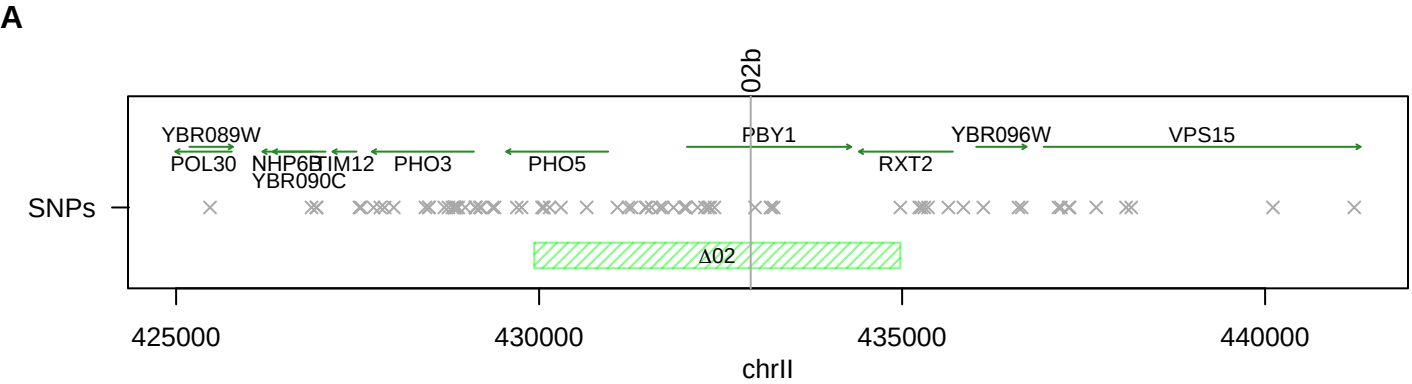
A
02b
YBR089W
POL30
NHP6B
YBR090C
TIM12
PHO3
PHO5
PBY1
RXT2
YBR096W
VPS15
SNPs
Δ02
425000
430000
435000
440000
chrII

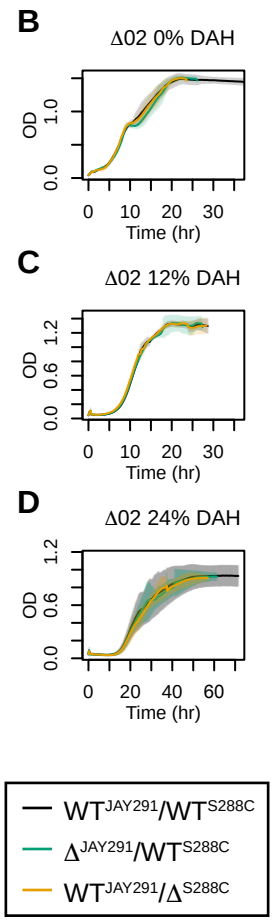
B
Δ02 0% DAH
OD
0.0
1.0
0
10
20
30
Time (hr)
C
Δ02 12% DAH
OD
0.0
0.6
1.2
0
10
20
30
Time (hr)
D
Δ02 24% DAH
OD
0.0
0.6
1.2
0
20
40
60
Time (hr)
WT^JAY291/WT^S288C
Δ^JAY291/WT^S288C
WT^JAY291/Δ^S288C

Figure S12

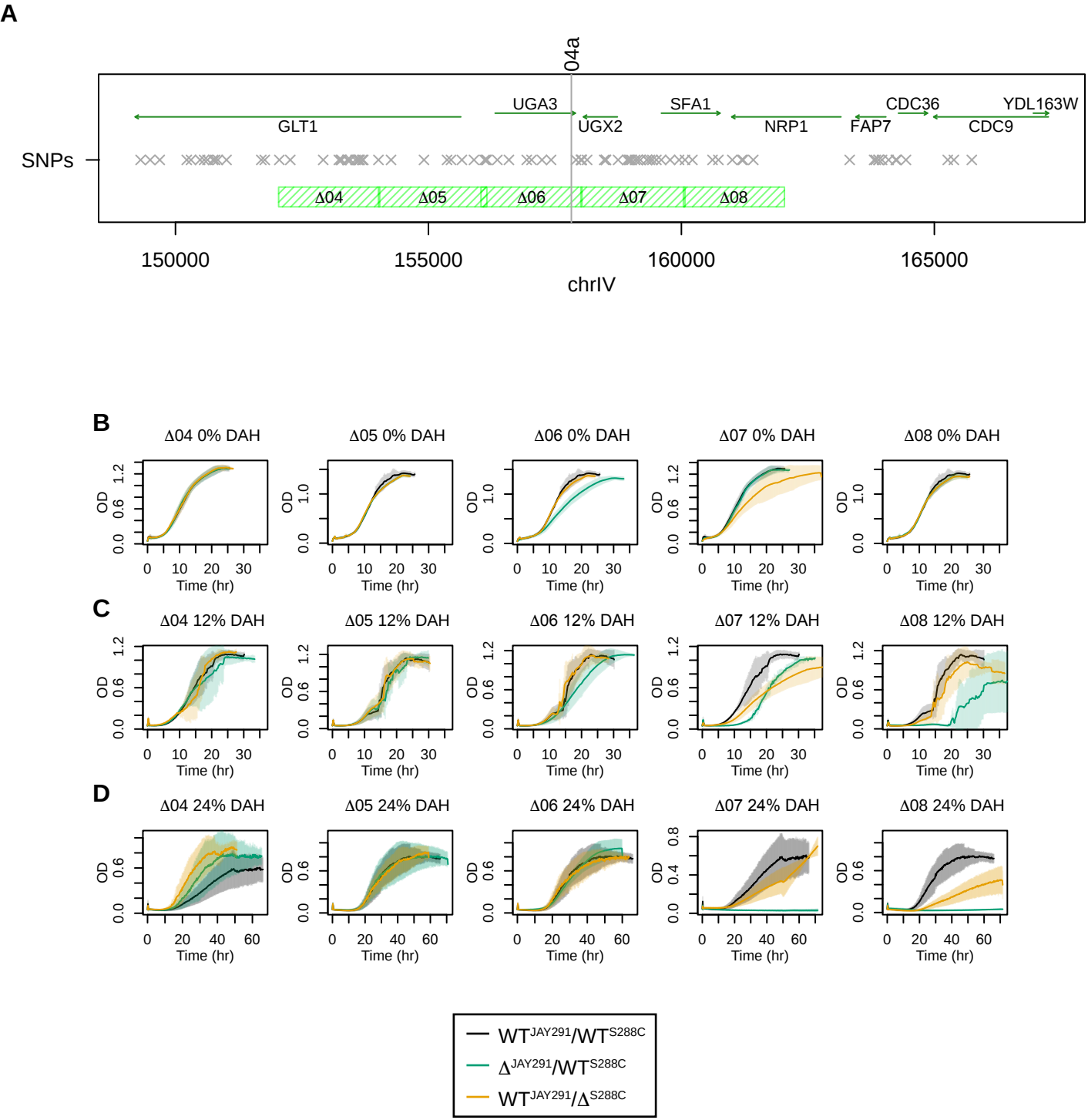
A
04a
GLT1
UGA3
UGX2
SFA1
NRP1
CDC36
FAP7
YDL163W
CDC9
SNPs
Δ04
Δ05
Δ06
Δ07
Δ08
150000
155000
160000
165000
chrIV
B
Δ04 0% DAH
Δ05 0% DAH
Δ06 0% DAH
Δ07 0% DAH
Δ08 0% DAH
C
Δ04 12% DAH
Δ05 12% DAH
Δ06 12% DAH
Δ07 12% DAH
Δ08 12% DAH
D
Δ04 24% DAH
Δ05 24% DAH
Δ06 24% DAH
Δ07 24% DAH
Δ08 24% DAH
OD
Time (hr)
WT^JAY291/WT^S288C
Δ^JAY291/WT^S288C
WT^JAY291/Δ^S288C

Figure S13

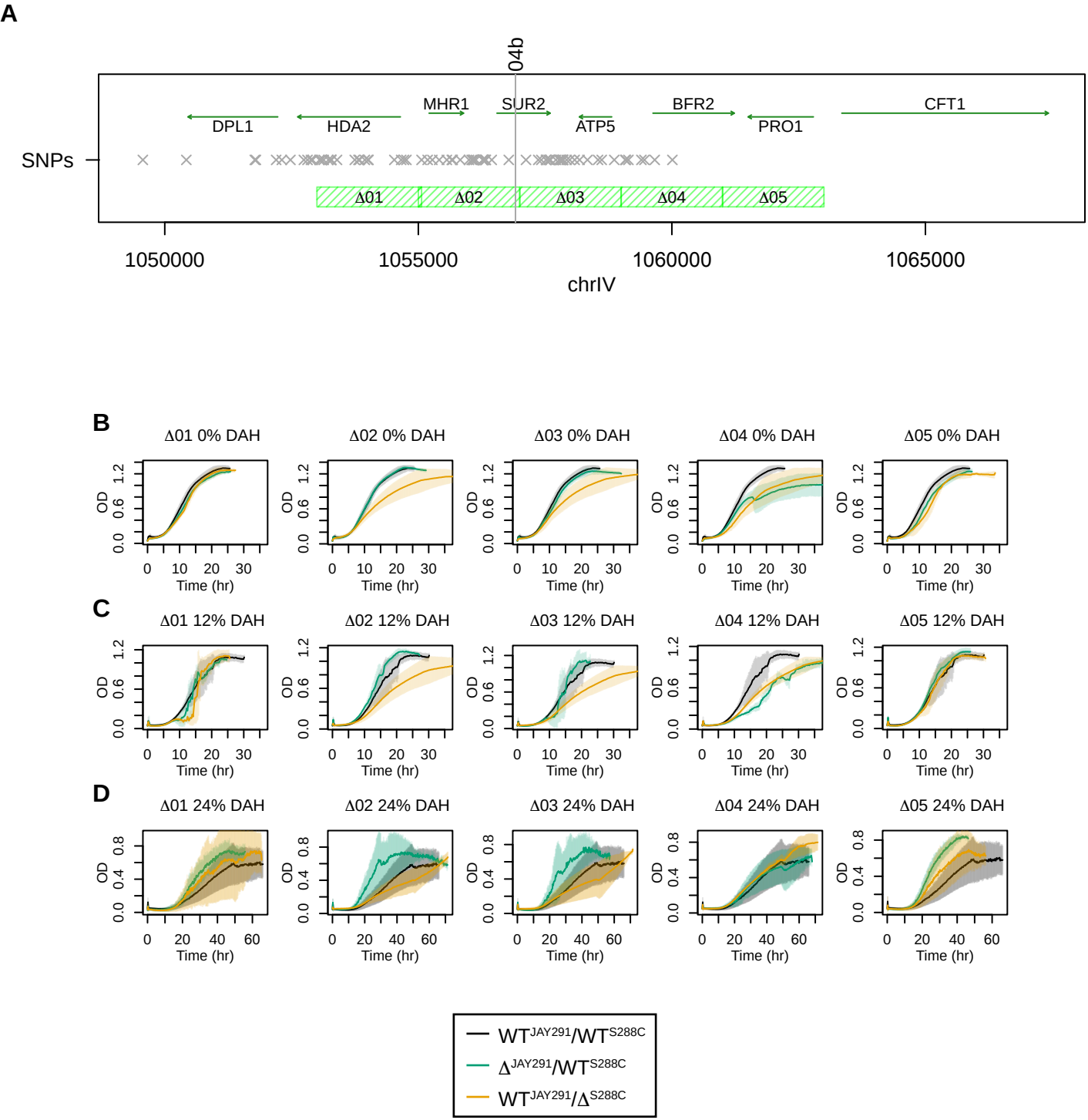
A
04b
DPL1
HDA2
MHR1
SUR2
ATP5
BFR2
PRO1
CFT1
SNPs
Δ01
Δ02
Δ03
Δ04
Δ05
1050000
1055000
1060000
1065000
chrIV
B
Δ01 0% DAH
Δ02 0% DAH
Δ03 0% DAH
Δ04 0% DAH
Δ05 0% DAH
C
Δ01 12% DAH
Δ02 12% DAH
Δ03 12% DAH
Δ04 12% DAH
Δ05 12% DAH
D
Δ01 24% DAH
Δ02 24% DAH
Δ03 24% DAH
Δ04 24% DAH
Δ05 24% DAH
OD
Time (hr)
WT^JAY291/WT^S288C
Δ^JAY291/WT^S288C
WT^JAY291/Δ^S288C

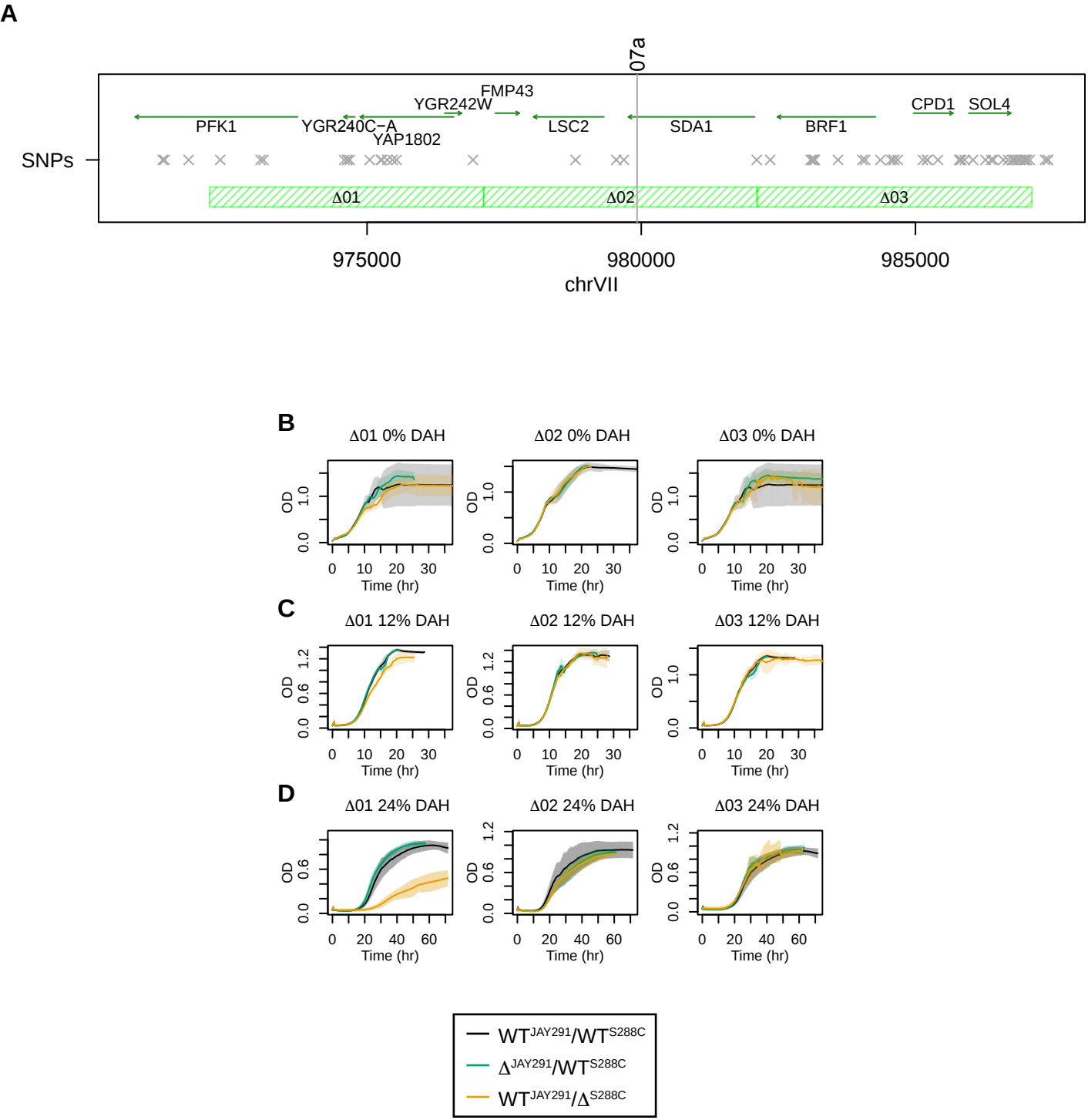
A
07a
FMP43
YGR242W
CPD1
SOL4
PFK1
YGR240C−A
YAP1802
LSC2
SDA1
BRF1
SNPs
Δ01
Δ02
Δ03
975000
980000
985000
chrVII
B
Δ01 0% DAH
Δ02 0% DAH
Δ03 0% DAH
C
Δ01 12% DAH
Δ02 12% DAH
Δ03 12% DAH
D
Δ01 24% DAH
Δ02 24% DAH
Δ03 24% DAH
OD
Time (hr)
WT^JAY291/WT^S288C
Δ^JAY291/WT^S288C
WT^JAY291/Δ^S288C

Figure S15

A

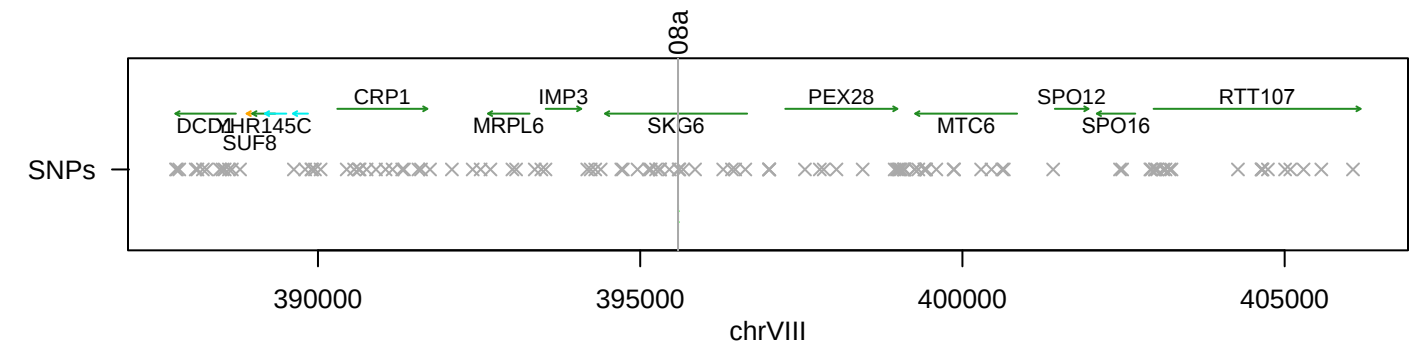

No bRHA strains were analyzed for this QTL region

Figure S16

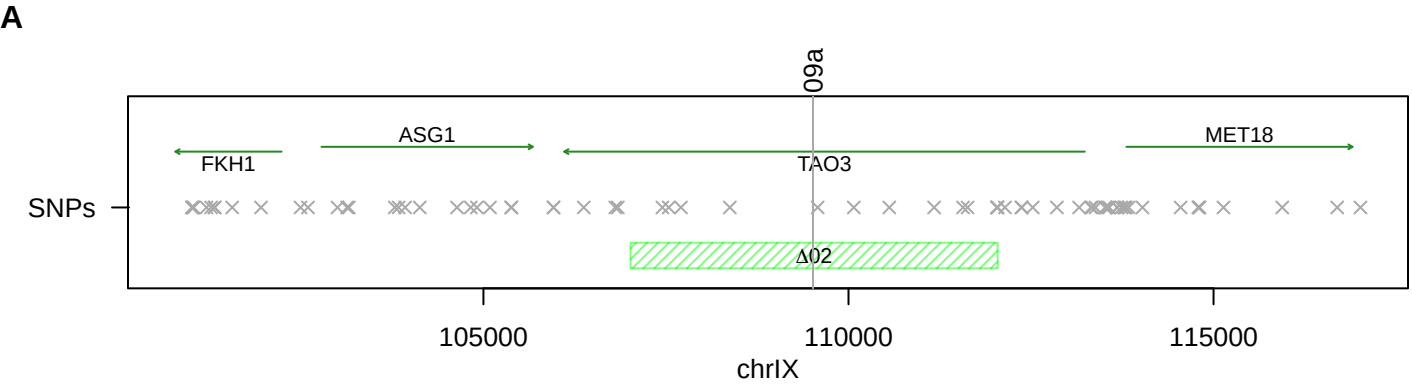
A
09a
ASG1
FKH1
TAO3
MET18
SNPs
Δ02
105000
110000
115000
chrIX

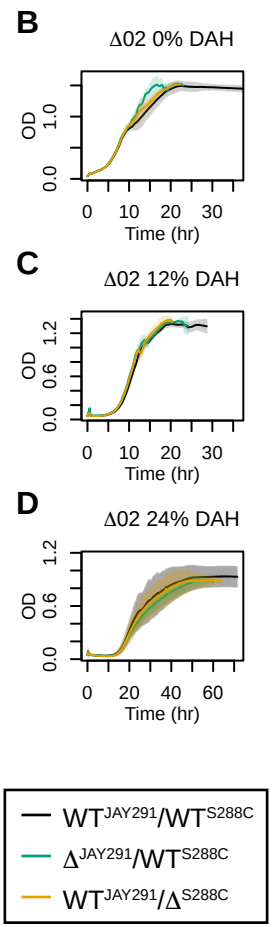
B
Δ02 0% DAH
OD
0.0
1.0
0
10
20
30
Time (hr)
C
Δ02 12% DAH
OD
0.0
0.6
1.2
0
10
20
30
Time (hr)
D
Δ02 24% DAH
OD
0.0
0.6
1.2
0
20
40
60
Time (hr)
WT^JAY291/WT^S288C
Δ^JAY291/WT^S288C
WT^JAY291/Δ^S288C

Figure S17

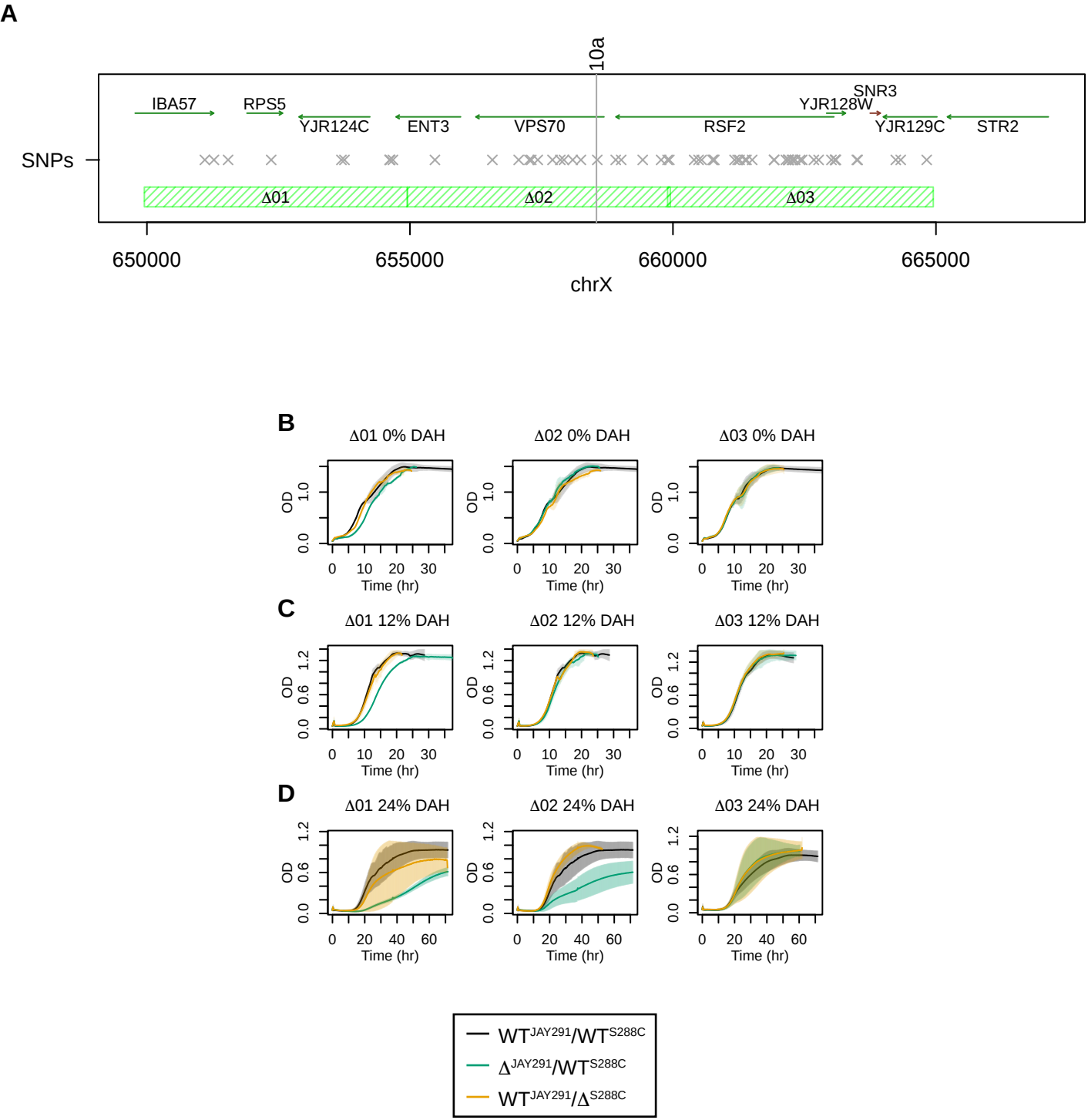
A
10a
IBA57
RPS5
YJR124C
ENT3
VPS70
RSF2
YJR128W
SNR3
YJR129C
STR2
SNPs
Δ01
Δ02
Δ03
650000
655000
660000
665000
chrX
B
Δ01 0% DAH
Δ02 0% DAH
Δ03 0% DAH
C
Δ01 12% DAH
Δ02 12% DAH
Δ03 12% DAH
D
Δ01 24% DAH
Δ02 24% DAH
Δ03 24% DAH
OD
Time (hr)
WT^JAY291/WT^S288C
Δ^JAY291/WT^S288C
WT^JAY291/Δ^S288C

Figure S18

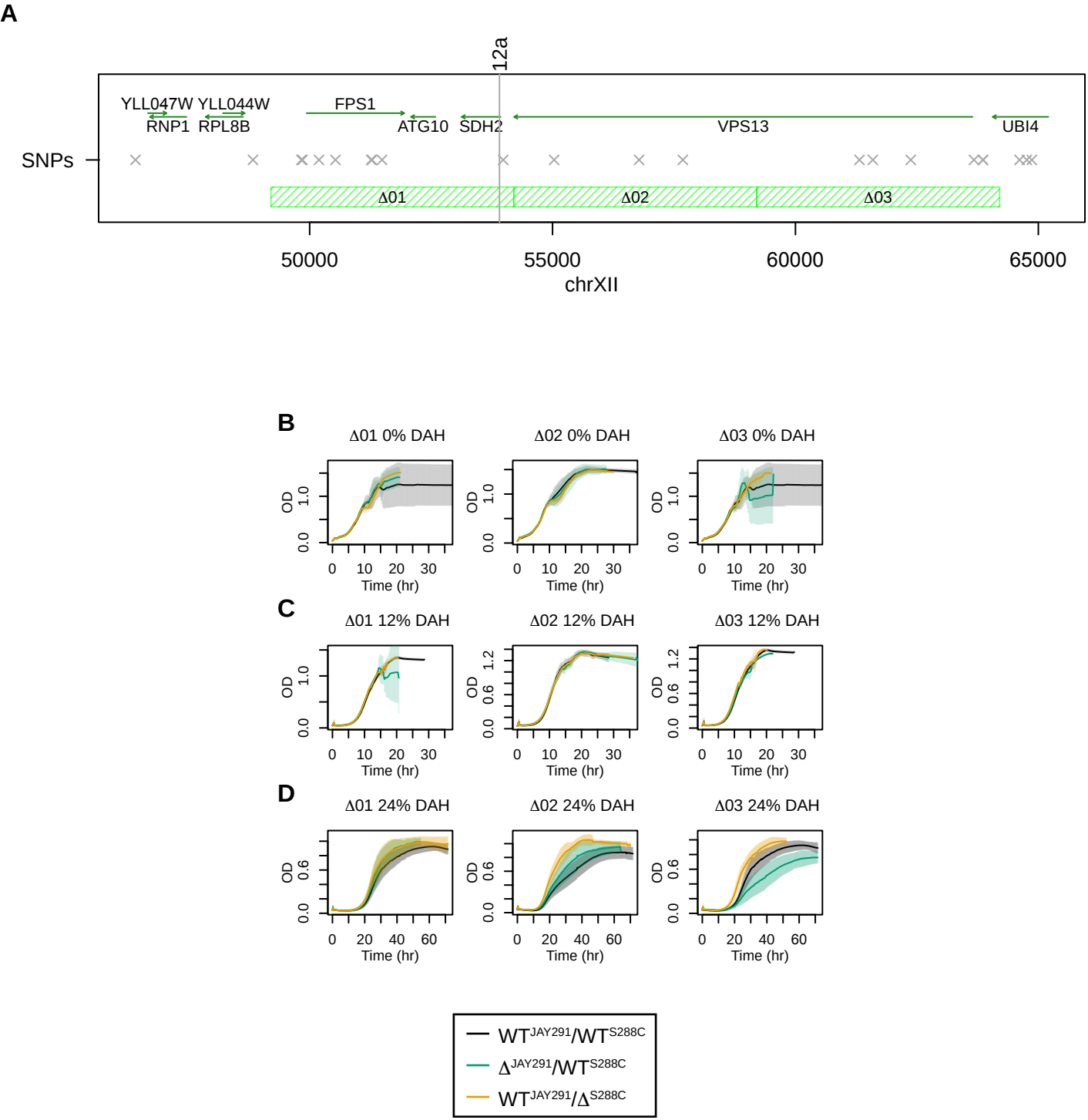
A
12a
YLL047W YLL044W
RNP1 RPL8B
FPS1
ATG10
SDH2
VPS13
UBI4
SNPs
Δ01
Δ02
Δ03
50000
55000
60000
65000
chrXII
B
Δ01 0% DAH
Δ02 0% DAH
Δ03 0% DAH
C
Δ01 12% DAH
Δ02 12% DAH
Δ03 12% DAH
D
Δ01 24% DAH
Δ02 24% DAH
Δ03 24% DAH
OD
Time (hr)
WT^JAY291/WT^S288C
Δ^JAY291/WT^S288C
WT^JAY291/Δ^S288C

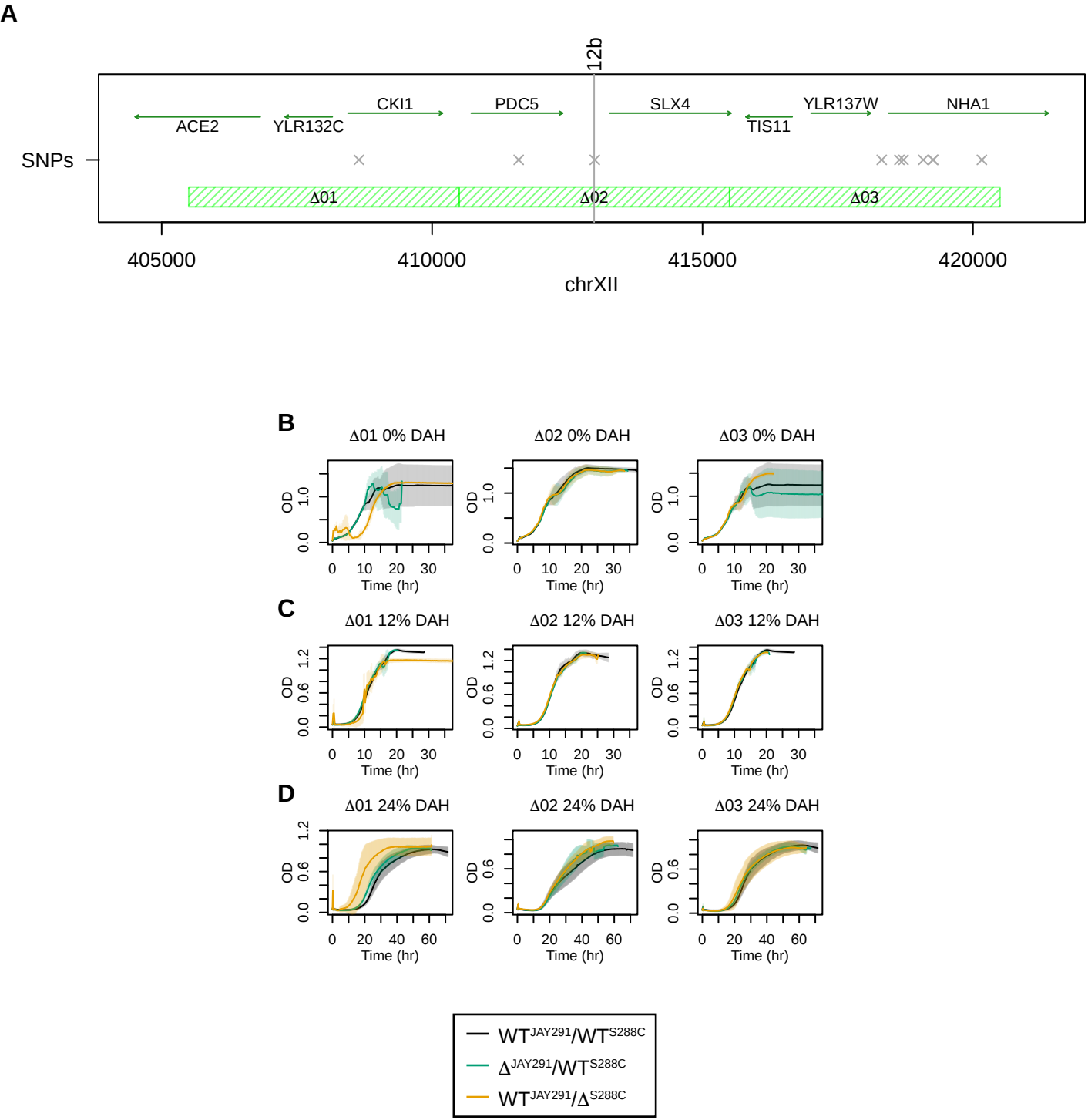
A
12b
ACE2
YLR132C
CKI1
PDC5
SLX4
TIS11
YLR137W
NHA1
SNPs
Δ01
Δ02
Δ03
405000
410000
415000
420000
chrXII
B
Δ01 0% DAH
Δ02 0% DAH
Δ03 0% DAH
C
Δ01 12% DAH
Δ02 12% DAH
Δ03 12% DAH
D
Δ01 24% DAH
Δ02 24% DAH
Δ03 24% DAH
OD
Time (hr)
WT^JAY291/WT^S288C
Δ^JAY291/WT^S288C
WT^JAY291/Δ^S288C

Figure S20

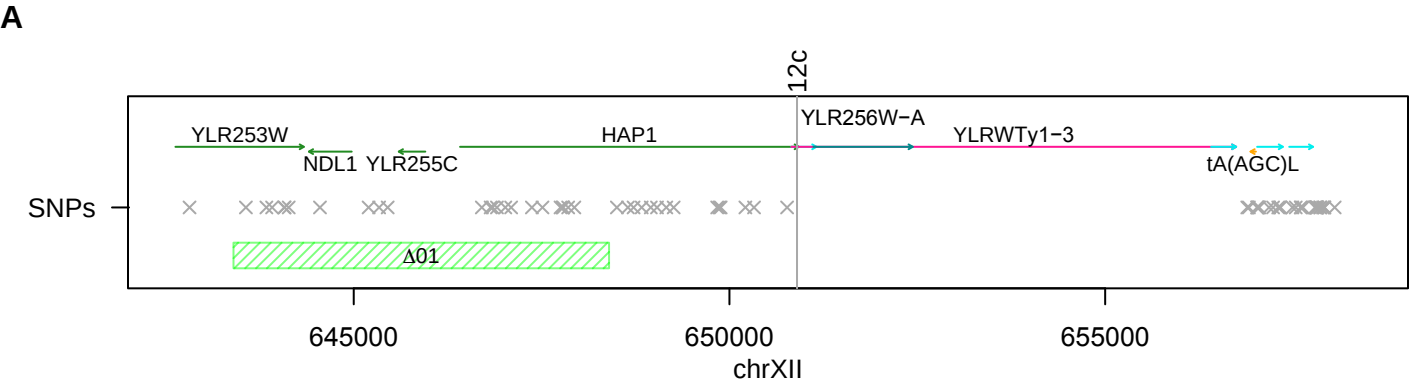
A
12c
YLR253W
NDL1
YLR255C
HAP1
YLR256W−A
YLRWTy1−3
tA(AGC)L
SNPs
Δ01
645000
650000
655000
chrXII

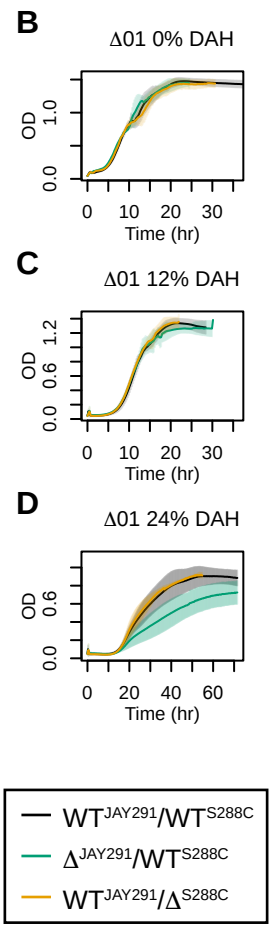
B
Δ01 0% DAH
OD
0.0
1.0
0
10
20
30
Time (hr)
C
Δ01 12% DAH
OD
0.0
0.6
1.2
0
10
20
30
Time (hr)
D
Δ01 24% DAH
OD
0.0
0.6
0
20
40
60
Time (hr)
WT^JAY291/WT^S288C
Δ^JAY291/WT^S288C
WT^JAY291/Δ^S288C

Figure S21

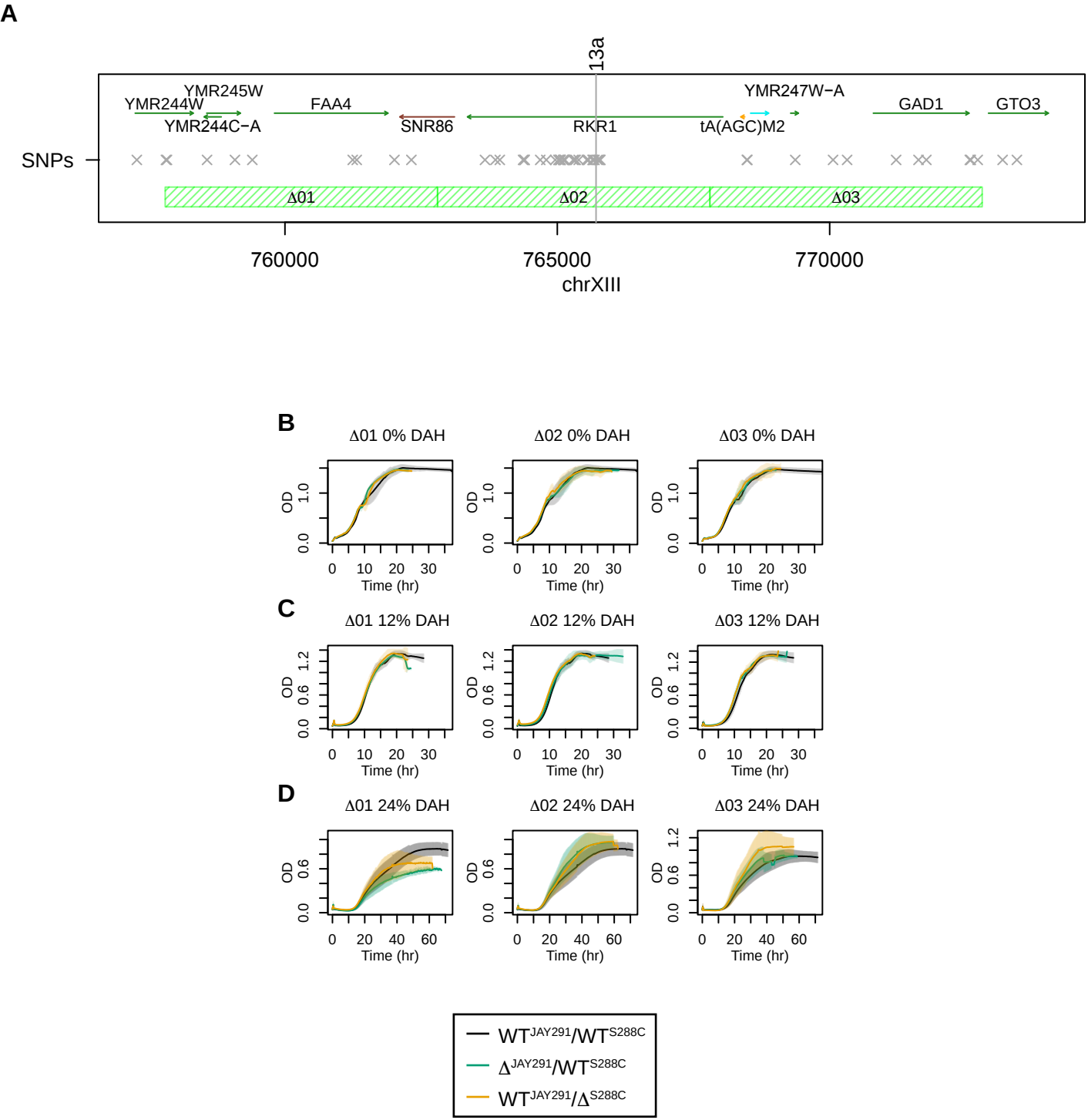
A
13a
YMR245W
YMR244W
YMR244C−A
FAA4
SNR86
RKR1
YMR247W−A
tA(AGC)M2
GAD1
GTO3
SNPs
Δ01
Δ02
Δ03
760000
765000
770000
chrXIII
B
Δ01 0% DAH
Δ02 0% DAH
Δ03 0% DAH
C
Δ01 12% DAH
Δ02 12% DAH
Δ03 12% DAH
D
Δ01 24% DAH
Δ02 24% DAH
Δ03 24% DAH
OD
Time (hr)
WT^JAY291/WT^S288C
Δ^JAY291/WT^S288C
WT^JAY291/Δ^S288C

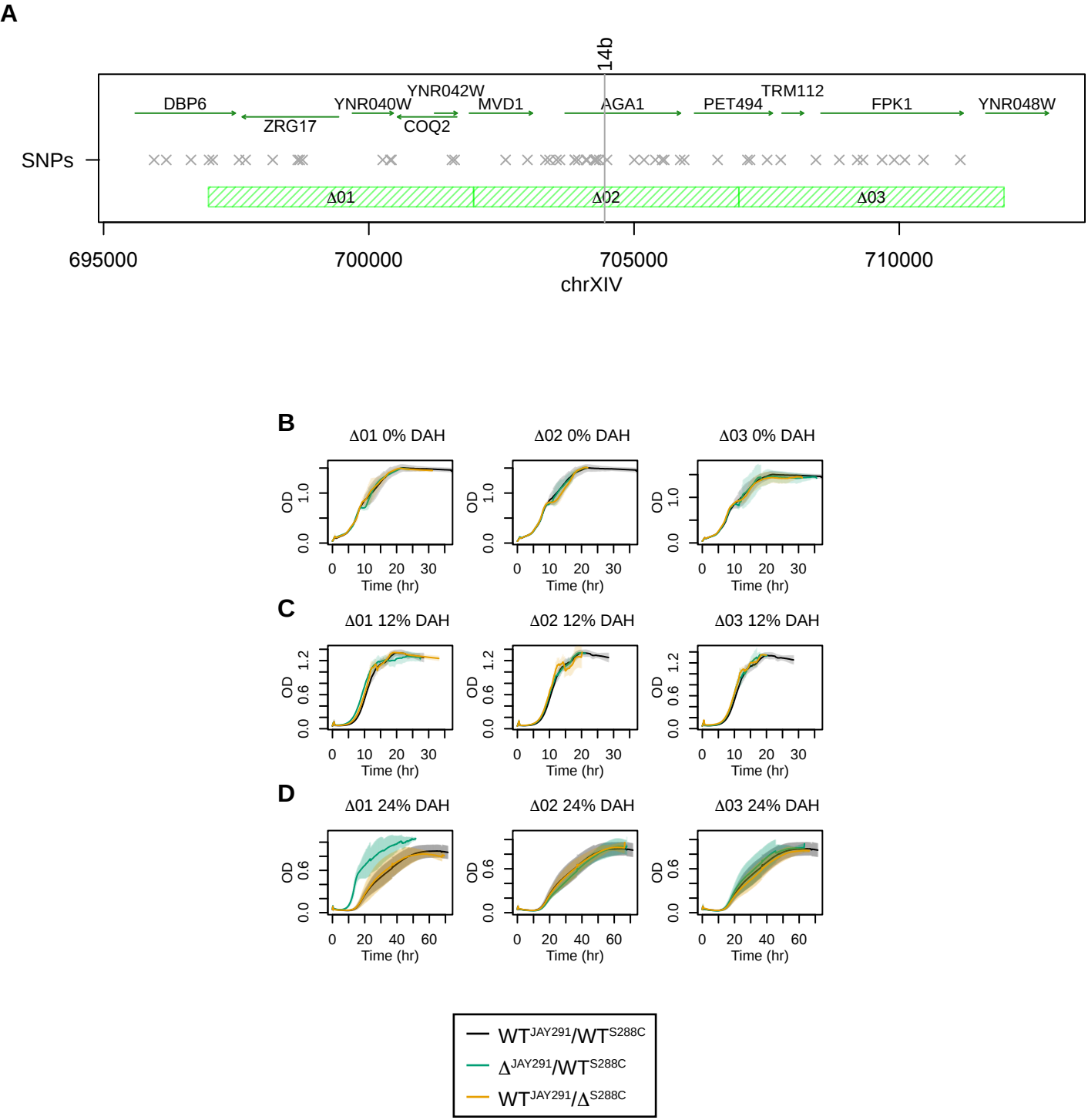
A
14b
DBP6
ZRG17
YNR040W
YNR042W
COQ2
MVD1
AGA1
PET494
TRM112
FPK1
YNR048W
SNPs
Δ01
Δ02
Δ03
695000
700000
705000
710000
chrXIV
B
Δ01 0% DAH
Δ02 0% DAH
Δ03 0% DAH
C
Δ01 12% DAH
Δ02 12% DAH
Δ03 12% DAH
D
Δ01 24% DAH
Δ02 24% DAH
Δ03 24% DAH
OD
Time (hr)
WT^JAY291/WT^S288C
Δ^JAY291/WT^S288C
WT^JAY291/Δ^S288C

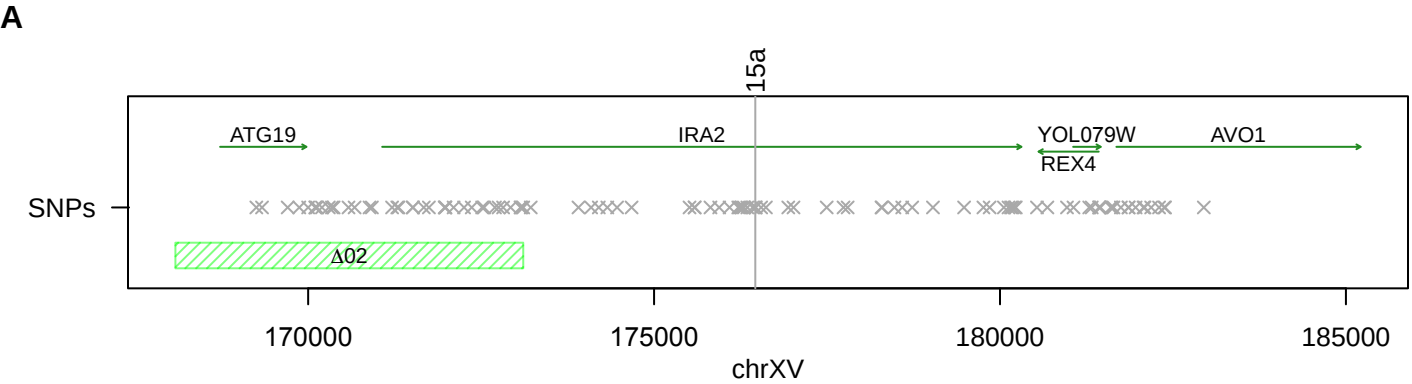
A
15a
ATG19
IRA2
YOL079W
AVO1
REX4
SNPs
Δ02
170000
175000
180000
185000
chrXV

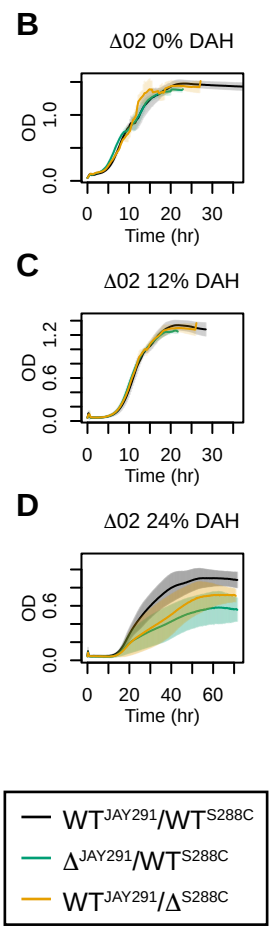
B
Δ02 0% DAH
OD
0.0
1.0
0
10
20
30
Time (hr)
C
Δ02 12% DAH
OD
0.0
0.6
1.2
0
10
20
30
Time (hr)
D
Δ02 24% DAH
OD
0.0
0.6
0
20
40
60
Time (hr)
WT^JAY291/WT^S288C
Δ^JAY291/WT^S288C
WT^JAY291/Δ^S288C

Figure S24

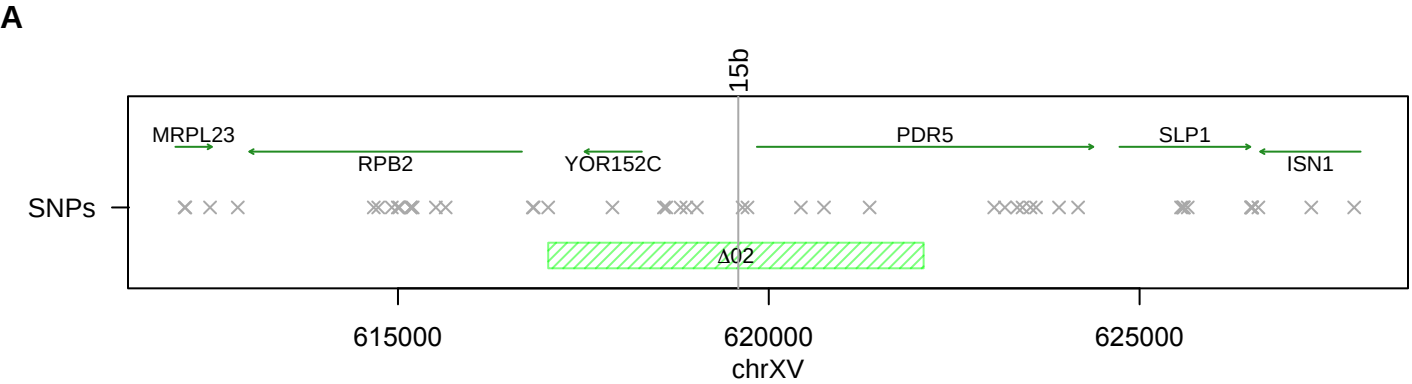
A
15b
MRPL23
RPB2
YOR152C
PDR5
SLP1
ISN1
SNPs
Δ02
615000
620000
625000
chrXV

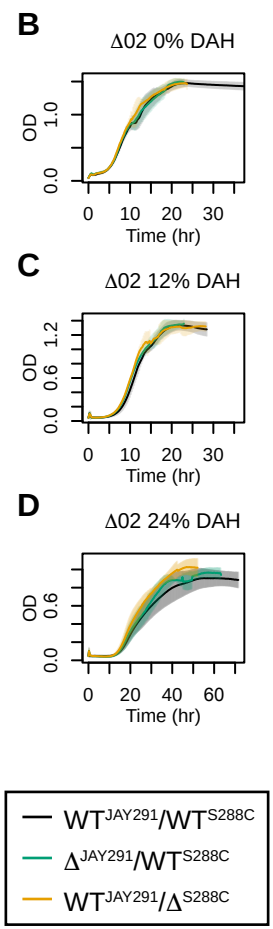
B
Δ02 0% DAH
C
Δ02 12% DAH
D
Δ02 24% DAH
OD
Time (hr)
WT^JAY291/WT^S288C
Δ^JAY291/WT^S288C
WT^JAY291/Δ^S288C

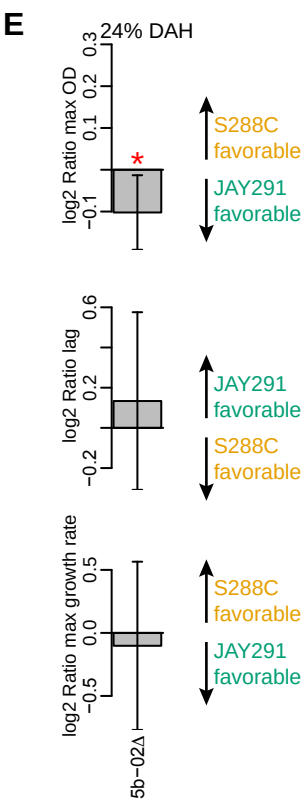
E
24% DAH
log2 Ratio max OD
log2 Ratio lag
log2 Ratio max growth rate
S288C favorable
JAY291 favorable
15b−02Δ

Figure S25

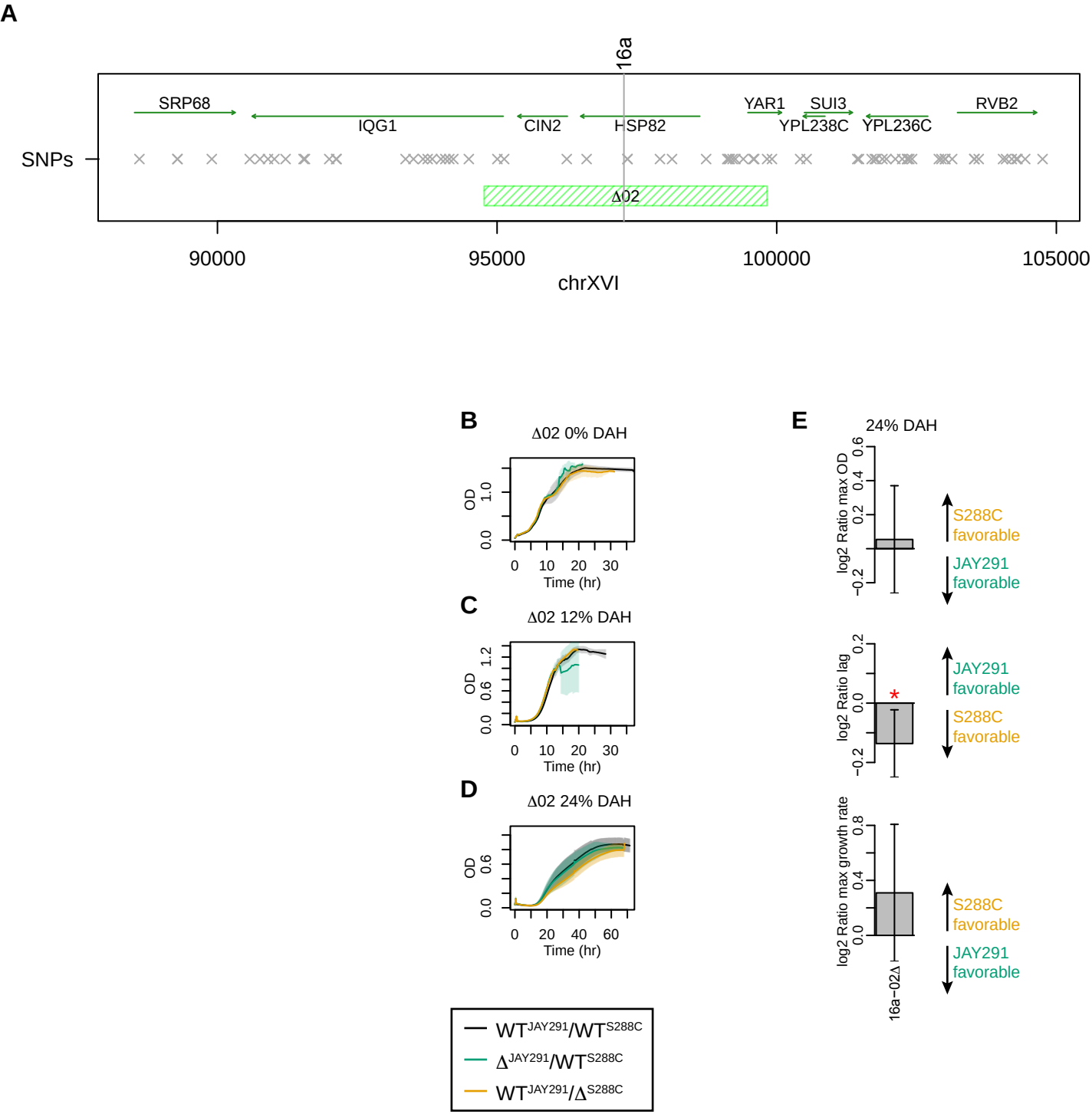
A
16a
SRP68
IQG1
CIN2
HSP82
YAR1
SUI3
YPL238C
YPL236C
RVB2
SNPs
Δ02
90000
95000
100000
105000
chrXVI
B
Δ02 0% DAH
OD
Time (hr)
C
Δ02 12% DAH
D
Δ02 24% DAH
E
24% DAH
log2 Ratio max OD
S288C favorable
JAY291 favorable
log2 Ratio lag
log2 Ratio max growth rate
16a−02Δ
WT^JAY291/WT^S288C
Δ^JAY291/WT^S288C
WT^JAY291/Δ^S288C